JGP Journal of General Physiology

COMMUNICATION

Protein phosphorylation maintains the normal function of cloned human $Ca_v2.3$ channels

Felix Neumaier, Serdar Alpdogan, Jürgen Hescheler, and Toni Schneider

R-type currents mediated by native and recombinant $Ca_v2.3$ voltage-gated Ca^{2+} channels (VGCCs) exhibit facilitation (run-up) and subsequent decline (run-down) in whole-cell patch-clamp recordings. A better understanding of the two processes could provide insight into constitutive modulation of the channels in intact cells, but low expression levels and the need for pharmacological isolation have prevented investigations in native systems. Here, to circumvent these limitations, we use conventional and perforated-patch-clamp recordings in a recombinant expression system, which allows us to study the effects of cell dialysis in a reproducible manner. We show that the decline of currents carried by human $Ca_v2.3+\beta_3$ channel subunits during run-down is related to adenosine triphosphate (ATP) depletion, which reduces the number of functional channels and leads to a progressive shift of voltage-dependent gating to more negative potentials. Both effects can be counteracted by hydrolysable ATP, whose protective action is almost completely prevented by inhibition of serine/threonine but not tyrosine or lipid kinases. Protein kinase inhibition also mimics the effects of run-down in intact cells, reduces the peak current density, and hyperpolarizes the voltage dependence of gating. Together, our findings indicate that ATP promotes phosphorylation of either the channel or an associated protein, whereas dephosphorylation during cell dialysis results in run-down. These data also distinguish the effects of ATP on $Ca_v2.3$ channels from those on other VGCCs because neither direct nucleotide binding nor PIP_2 synthesis is required for protection from run-down. We conclude that protein phosphorylation is required for $Ca_v2.3$ channel function and could directly influence the normal features of current carried by these channels. Curiously, some of our findings also point to a role for leupeptin-sensitive proteases in run-up and possibly ATP protection from run-down. As such, the present study provides a reliable baseline for further studies on $Ca_v2.3$ channel regulation by protein kinases, phosphatases, and possibly proteases.

Introduction

Electrophysiological recordings from excised cell patches or dialyzed cells are almost invariably hampered by time-dependent changes in voltage-gated ion channel function. The most common form of these phenomena, termed run-down or washout, is a progressive decline of ionic currents and is thought to reflect changes in intracellular signaling cascades, which occur secondary to the loss or dilution of cytosolic factors (Becq, 1996). It can be preceded by a transient current facilitation (run-up), which may reflect voltage- and time-dependent repriming (i.e., recovery from inactivation) or modification of signaling cascades that tonically inhibit these currents (Tiaho et al., 1993; Elhamdani et al., 1994, 1995). Although run-down remains a major obstacle for studies on voltage-gated Ca^{2+} channel (VGCC) function, it has also provided insight into the manifold regulation of these channels in intact cells. For example, the decline of L-type Ca^{2+} currents has been linked to several interrelated processes, which may include loss of ATP and other cytoplasmic factors, progressive protein dephosphorylation, decoupling of guanosine-5′-triphosphate (GTP)–binding proteins, and possibly increased proteolysis of the channels (Chad et al., 1987; McDonald et al., 1994; Kepplinger and Romanin, 2005; Xu et al., 2016; Yu et al., 2016). In P/Q-, N-, and certain neuronal L-type Ca^{2+} channels on the other hand, run-down appears to involve depletion of membrane PIP_2, a mechanism also thought to mediate M_1 muscarinic receptor-dependent inhibition of these channels (Wu et al., 2002; Suh et al., 2010). Much less is known about the run-down of "pharmaco-resistant" R-type currents, which are mainly mediated by $Ca_v2.3$-type VGCCs. R-type and R-type–like currents have been shown to exhibit both run-up and run-down (Cota, 1986; Hilaire et al., 1997; Benquet et al., 1999; Almog and Korngreen, 2009), but low expression levels and the need for pharmacological isolation have generally prevented further characterization of the

Institute for Neurophysiology, University of Cologne, Cologne, Germany.

Correspondence to Felix Neumaier: felix@neumaier-net.de.

two processes in native cells. The human embryonic kidney (HEK-293) cell line is widely used for heterologous expression of recombinant ion channels and receptors because it contains few endogenous channels, whereas most signaling pathways for regulation and posttranslational processing are operational (Toth et al., 1996; Thomas and Smart, 2005; Clare, 2006). Apart from circumventing the need for R-type current isolation, HEK-293 cells have a simple and uniform shape, which facilitates reproducible manipulation of their intracellular milieu. We therefore used conventional and perforated-patch-clamp recordings together with different inhibitors and cytosolic factors to study the effects of cell dialysis in a stably transfected HEK-293 cell line expressing human $Ca_v2.3+\beta_3$ channel subunits. Our findings show that the decline of macroscopic currents during run-down can partly be accounted for by changes in channel voltage dependence and that it can be prevented or slowed down by provision of intracellular ATP and in perforated-patch recordings. Protection from run-down depended on ATP-hydrolysis and was not related to lipid kinase-mediated PIP_2 synthesis or phosphorylation of tyrosine residues but was sensitive to inhibition of serine/threonine kinases. Protein kinase inhibition in intact cells also reduced peak current densities and reproduced the effects of run-down on channel voltage-dependence. Together, these findings indicate that run-down involves constitutive dephosphorylation of sites on the channels themselves or an associated protein and that ATP promotes phosphorylation of these sites by one or more endogenous kinases. Interestingly, our findings also indicate that the current facilitation during run-up could involve activation of leupeptin (Leu)-sensitive proteases, which may also influence the protective action of ATP.

Materials and methods

Cell culture

Human embryonic kidney (HEK-293) cells stably transfected with human $Ca_v2.3d$ and β_3 Ca^{2+} channel subunits (Nakashima et al., 1998) were cultured under normal growth conditions (37°C and 5% CO_2) in Dulbecco's modified Eagle medium (DMEM; Sigma-Aldrich) supplemented with 10% FCS and antibiotics (1% penicillin–streptomycin and selection markers: 1 mg/ml geneticin [G-418] and 200 µg/ml hygromycin B). Cells were routinely passaged twice a week by using 0.05% trypsin/0.02% EDTA. For electrophysiological recordings, cells were seeded on nitric acid–washed glass coverslips and used within 24–48 h after plating.

Electrophysiological recordings

Cells were voltage-clamped by using the whole-cell configuration of the patch-clamp technique (Hamill et al., 1981). Pipettes were prepared from thick-walled borosilicate glass capillaries (1.5/0.84-mm-outside/inside diameter; World Precision Instruments) by using a P97 Micropipette puller (Sutter Instruments). Resistance of the resulting electrodes was between 1.5 and 6.5 MΩ (mean = 3.8 ± 0.1 MΩ in 339 recordings) when filled with standard internal solution. The bath was connected to ground via 140 mM sodium chloride agar bridges. Currents were sampled at 20 or 50 kHz and filtered at 10 kHz by using an EPC9 amplifier (HEKA) controlled with HEKA's Pulse software. Leak and capacitive currents were subtracted online by use of a −P/5 protocol. Recordings obtained with voltage ramps were leak-corrected by a linear fit to the current recorded between −80 and −50 mV, which was extrapolated to +60 mV and subtracted from the whole recording. Series resistance (R_s) was compensated electronically by up to 90% (mean R_s after compensation = 2.7 ± 0.1 MΩ) and continuously monitored throughout the measurements. The charging time-constant after compensation was always ≤100 µs (mean = 38 ± 1 µs), and the maximum uncompensated R_s-error at the time of peak current was ≤2.5 mV (mean = 0.82 ± 0.04 mV). All experiments were performed at room temperature, from a holding potential of −80 mV and, unless noted otherwise, in cells with a whole-cell capacitance (C_s) between 5 and 25 pF (mean = 15 ± 1 pF), as estimated from the slow capacitance compensation of the amplifier. Perforated patch recordings were performed by using β-escin, which was dissolved in type I ultrapure water to prepare a 25 mM stock solution, protected from light and stored at −20°C for up to 2 wk. Before the recordings, aliquots of the stock solution were diluted in standard internal solution and vortex-mixed for 1 min to give a final escin concentration of 40 µM. After patch formation, gradual perforation was observed as a progressive increase in the speed and amplitude of capacitive transients during 5-ms voltage-steps to −75 mV. Cells showing signs of spontaneous patch rupture (i.e., sudden increase in the amplitude and speed of capacitive transients) were omitted or used as control recordings to exclude that β-escin itself affected the channel properties or the time course of changes in I_{Ba}.

Recording solutions and drugs

All solutions for electrophysiological experiments were prepared by using type 1 ultrapure water (Milli-Q by Millipore Corporation or Purelab Flex 2 by ELGA Labwater) and, unless noted otherwise, reagents purchased from Sigma-Aldrich. During the recordings, cells were constantly perfused with external solution containing (mM) 120 NaCl, 5 $BaCl_2$ or $CaCl_2$, 5 KCl, 1 $MgCl_2$, 20 TEA chloride, 10 glucose, 10 HEPES, and 0.1 BaEDTA with the pH adjusted to 7.4 by using NaOH and osmolarity of 300–320 mOsm. The solution was filtered through 0.2-µm polyethersulfone membranes and applied to cells at a rate of ∼2–4 ml/min by using a gravity-driven perfusion system controlled by manual precision flow regulators (Sarstedt). The standard intracellular solution was composed of (mM) 130 CsCl, 5 oxaloacetic acid, 5 creatine, 5 pyruvic acid, 10 EGTA, and 10 HEPES with the pH adjusted to 7.3 by using CsOH and osmolarity of 275–295 mOsm. It was stored at −20°C, thawed on the day of the experiments, filtered through 0.2-µm surfactant-free cellulose acetate membranes (Corning), and kept on ice between the recordings. The liquid junction potential between internal and external solution (calculated by using the JPcalc algorithm in pClamp 10; Molecular Devices) was ∼5.5 mV. Because no correction for the liquid junction potential was done, all voltages shown were actually 5.5 mV more negative.

Nucleotide triphosphates (NaATP, MgATP, and MgGTP) were dissolved in 10 mM HEPES to prepare 100 mM stock solutions (pH = 7.3), stored at −20°C and diluted in standard internal solution immediately before the recordings. Calmodulin (CaM) was dissolved in type I ultrapure water to prepare a 100 µM stock solution and stored at −20°C. AMP-PNP was used as the lithium

salt and dissolved directly in the standard internal solution. Deltamethrin, wortmannin, U73122, genistein, and staurosporine (stauro) were dissolved in DMSO to prepare 2–50 mM stock solutions, protected from light and stored at −20°C. Before the experiments, they were diluted in standard internal solution, and the same amount of DMSO (0.1–0.25% vol/vol) without drug was added to the internal solution used for parallel control recordings. To account for the short half-life in aqueous media, all solutions containing wortmannin were discarded after a maximum of 20 min after its dilution into standard internal or external solution, respectively. Cytosolic extract was prepared on the day of the experiments by freeze/thaw lysis of ∼2.1×10^7 cells in 1.5 ml ice-cold pipette solution. After centrifugation at 0°C for 5 min, the supernatant was filtered through a 0.2-µm surfactant-free cellulose membrane (Corning), an aliquot was removed for quantification of the protein concentration, and the rest was immediately used for the recordings.

Whole-cell protocols

Unless noted otherwise, time-course recordings were performed by repetitive application at 0.03 Hz of a 30-ms test pulse to +10 mV followed by 10-ms repolarization at −50 mV to record well resolved tail-currents. In some experiments, a 50-ms voltage ramp from −80 mV to +60 mV (2.8 V/s) was used instead of the voltage steps to monitor changes in the quasi steady-state voltage dependence. Because recordings with drugs added to the internal solution could not be used as their own control, we always performed parallel control recordings with standard internal solution. To study changes in current immediately after establishing the whole-cell configuration, cells were clamped at the holding potential of −80 mV before disruption of the patch. After patch rupture, capacitance was quickly compensated by using the auto function of the amplifier, and stimulation started after a delay of no more than 10 s. Because initial current amplitudes were small and several seconds were often required for R_s to stabilize completely, the first response was always recorded without R_s compensation. We then stopped stimulation, adjusted the R_s compensation of the amplifier to achieve maximal compensation without ringing, and restarted the stimulation protocol. To reduce variation introduced by differences in the time required for stabilization of R_s, initial values (I_{start}) for statistical comparison were always calculated as the average of the first two responses, which also provided a compromise between the lack of R_s compensation during acquisition of the first response and the time that had already evolved when the second response was recorded. To construct steady-state current-voltage (IV) relationships, peak currents recorded with a protocol consisting of 25-ms test pulses to potentials between −80 mV and +60 mV (10-mV increments at 0.1 Hz) were normalized by the maximum current amplitude at time 0 and plotted as a function of the test-pulse potential. Instantaneous IV (IIV) relationships were obtained with a protocol consisting of a fixed 10-ms prepulse to +60 mV followed by 40-ms test pulses to potentials between −80 mV and +60 mV (10-mV increments at 0.1 Hz). Instantaneous (tail) current amplitudes recorded during the test pulses were normalized by the maximum tail current amplitude at time 0 and plotted as a function of the prepulse potential. The voltage dependence of activation was assessed by a protocol consisting of 25-ms prepulses to potentials between −80 mV and +60 mV (10-mV increments at 0.1 Hz) followed by a fixed 10-ms test pulse to −50 mV. Tail-current amplitudes recorded during the test pulse were normalized to the maximum tail-current amplitude and plotted as a function of the prepulse potential to construct isochronous activation curves. The fraction of channels available for activation from different holding potentials was assessed by a protocol consisting of 3-s conditioning prepulses at potentials between −120 mV and +10 mV (10-mV increments at 0.1 Hz) followed by a fixed 35-ms test pulse to +10 mV. To construct prepulse inactivation curves, peak current amplitudes recorded during the test pulse were normalized by the maximum amplitude and plotted as a function of the prepulse potential.

Data analysis and statistics

Leak-subtracted current traces were directly analyzed with PulseFit (HEKA) or exported for further processing with Microsoft Excel 2010 and OriginLab Pro (version 9; OriginLab).

Time-course recordings were quantified in terms of the current increase during run-up, the duration of run-up, and the residual current after 7 min of run-down, as detailed in the results section. To compare the effect of various test solutions, each of these parameters was also normalized by the mean value observed in parallel control recordings according to Eq. 1:

$$\Delta p_t = p_t - \overline{p_c}, \quad (1)$$

where p_t is the value of parameter p measured in a cell with test solution t, $\overline{p_c}$ is the mean value of p in parallel control recordings, and Δp_t is the normalized value of p, which should provide an estimate for the amount of change over control.

IV relationships were fitted with a combined Ohm-Boltzmann equation (Eq. 2):

$$I = (V_m - V_{rev}) * g_{IV} / (1 + \exp(-(V_m - V_{0.5})/k)), \quad (2)$$

where I is the (normalized) peak current density measured at the test potential V_m, V_{rev} is the apparent reversal potential, g_{IV} is the maximum slope conductance, $V_{0.5}$ is the voltage eliciting half-maximal inward currents, and k is the slope factor. Isochronous activation and prepulse inactivation curves were fitted with single Boltzmann equations (Eq. 3):

$$I/I_{max} = A_2 + (A_1 - A_2)/(1 + \exp((V_m - V_{0.5})/k)), \quad (3)$$

where I/I_{max} is the normalized current at the prepulse potential V_m, $V_{0.5}$ is the voltage of half-maximal activation ($V_{0.5act}$) or inactivation ($V_{0.5inact}$), k is the activation (k_{act}) or inactivation (k_{inact}) slope factor, and A_1 and A_2 are the initial and final values, respectively. All fits were performed by using the Levenberg-Marquardt least-squares algorithm, and the goodness of fit was judged based on residual plots and adjusted χ^2 values. Smooth curves in the figures represent fits to average data whereas values given in the text are average data from fits to individual measurements. Values in the text and figures are expressed as mean ± SEM based on the number of independent experiments. Statistical significance was assessed with OriginLab Pro 9 by using a repeated-measures ANOVA followed by Bonferroni's post hoc analysis when comparing mean values from

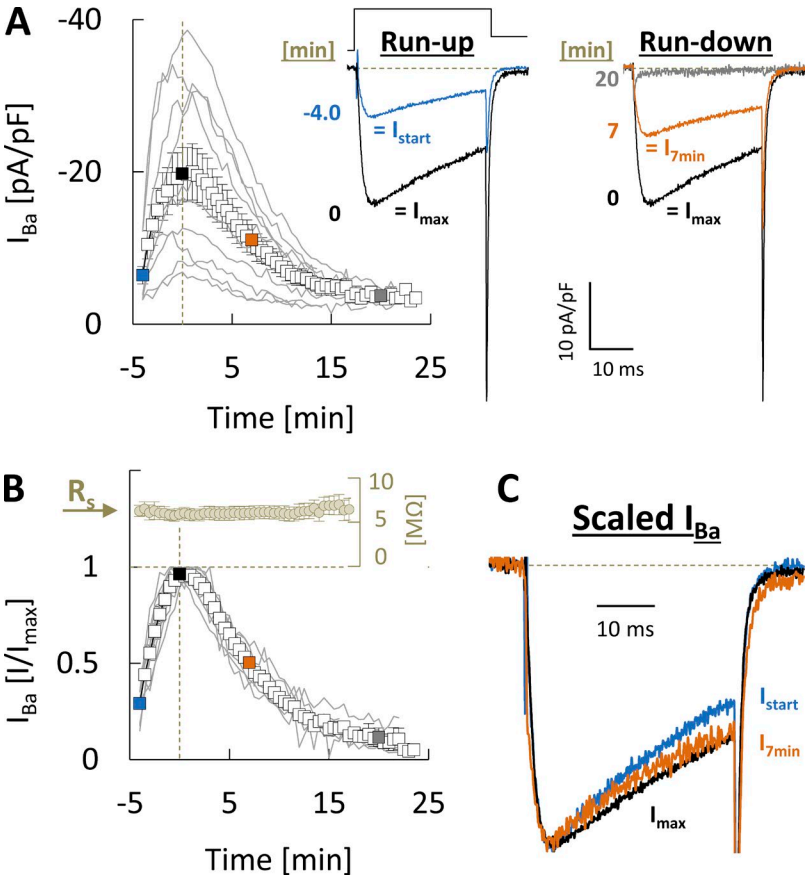

Figure 1. **Evolution and run-down of $Ca_v2.3$ channel currents carried by 5 mM Ba^{2+}. (A)** Time course of changes in peak whole-cell currents evoked by repetitive step depolarization to 10 mV every 30 s (n = 10). For consistency with the later figures, time 0 is defined as the time of maximum inward current (I_{max}). Gray lines in the background indicate time course of changes in individual recordings. Also shown are mean current traces corresponding to the time points indicated next to the traces and by filled symbols in the graph. **(B)** Same data as in A but normalized to the maximum peak current amplitude (I_{max}). Gray lines in the background indicate the time course of changes in individual recordings. Also shown above is the lack of spontaneous changes in R_s over the time course of the recordings. **(C)** Same current traces as in A but scaled to their maximum amplitude to visualize changes in their shape. Values are expressed as mean ± SEM.

the same cells or a one-way ANOVA followed by Bonferroni's post hoc analysis when comparing multiple independent mean values. Homogeneity of variances between groups was tested by using Levene's test for equality of variances on the squared deviations. In the case of heteroscedastic data ($P < 0.05$ in Levene's test and ratio of largest-to-smallest variance ≥4), statistical significance was assessed with Minitab (version 17; Minitab Inc.) by using Welch's ANOVA and the Games-Howell multiple-comparison method. The secondary $Ca_v2.3$ channel structure in Fig. 14 was visualized by using the web-based tool Protter for interactive protein feature visualization (available at http://wlab.ethz.ch/protter/start/; Omasits et al., 2014). Phosphorylation sites in the same figure were predicted at the highest threshold with the Group-based Prediction Software for Prediction of Kinase-specific Phosphorylation Sites 3.0 (available at http://gps.biocuckoo.org; Xue et al., 2008).

Results

Evolution and run-down of cloned $Ca_v2.3$ channel currents

Fig. 1 summarizes changes over time in macroscopic $Ca_v2.3$ channel currents carried by 5 mM Ba^{2+} and evoked by voltage-steps to 10 mV in dialyzed HEK-293 cells. Peak current amplitudes recorded immediately after establishing the whole-cell configuration (I_{start}) were small and tended to increase for several minutes (run-up) until they reached a maximum value (I_{max}). This was invariably followed by a progressive but somewhat slower current decline (run-down), so that the response that remained 7 min after complete run-up (I_{7min}) amounted to approximately half of the maximum current amplitude (Fig. 1, A and B).

We quantified the time course of changes by estimating (1) the time required after patch rupture for currents to reach I_{max} (= time to I_{max}), (2) the ratio between I_{max} and I_{start} (= increase), and (3) the ratio between I_{7min} and I_{max} (= remaining I_{Ba}). Under standard recording conditions (Fig. 1), with mean R_s and C_s values of 6 ± 1 MΩ and 14 ± 1 pF, respectively (n = 10), run-up took 4 ± 1 min and was associated with a 2.7 ± 0.2-fold increase of peak I_{Ba} at 10 mV, whereas the residual current amplitude after partial run-down amounted to 42 ± 4% of its maximum value.

As illustrated by inspection of scaled current traces (Fig. 1 C), the initial increase of currents was paralleled by a decrease of fractional inactivation during the 30-ms test-pulses from 53 ± 4% immediately after establishing the whole-cell configuration to 40 ± 4% ($P < 0.001$) after complete run-up. On the other hand, run-down tended to increase inactivation, although quantification of this effect was often confounded by the reduced signal-to-noise ratio due to current decline (but see also Fig. 13 E).

The general time course of changes was very similar among cells with different peak current densities, not attributable to voltage loss or R_s variation (Fig. 1 B) and unaffected by inclusion of two 3-min resting periods without stimulation (not depicted).

Factors involved in run-up and run-down

Increased mechanical tension associated with fluid flow has been shown to cause run-up and functional alterations in some other VGCCs (Peng et al., 2005; Park et al., 2007), but the time-dependent

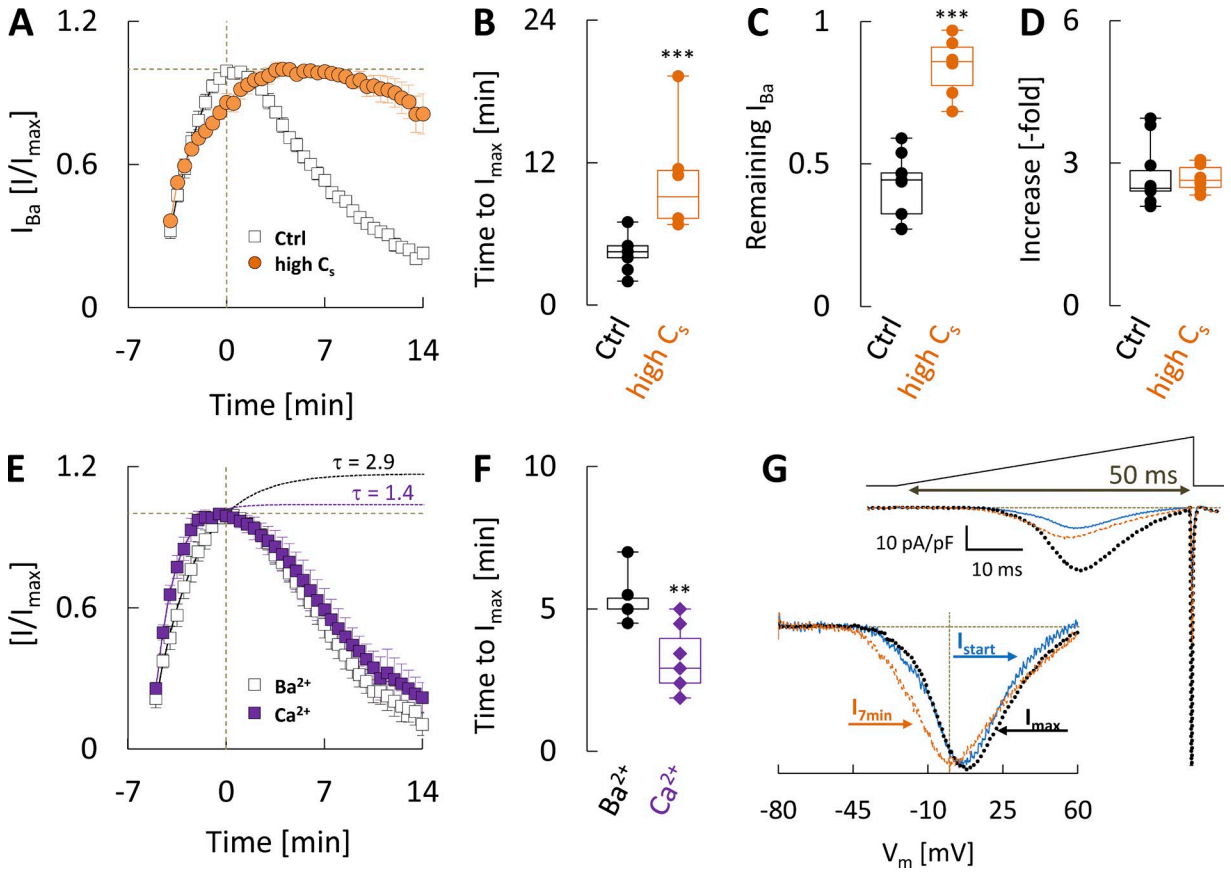

Figure 2. **Dependence of run-up and run-down on cell dialysis, Ca^{2+}, and voltage. (A)** Comparison of time-course recordings performed under standard recording conditions (Ctrl, with R_s = 6 ± 1 MΩ and C_s = 14 ± 1 pF; same data as in Fig. 1) or with high-resistance pipettes (R_s = 12 ± 1 MΩ) in large cells (C_s = 29 ± 6 pF) to retard cytosolic dilution (high C_s, *n* = 6). **(B)** Comparison of the run-up duration, determined as the time required for currents to reach their maximum amplitude (same cells as in A). **(C)** Comparison of the residual current after partial run-down, determined as the ratio between current amplitudes after 7 min of run-down and at time 0 (same cells as in A). **(D)** Comparison of the current increase during run-up, determined as the ratio between maximum and initial current amplitude (same cells as in A). **(E)** Comparison of time-course recordings performed with 5 mM Ba^{2+} (*n* = 5) or Ca^{2+} (*n* = 5) as the charge carrier. Dotted lines are extrapolated single exponential fits to the evolution of currents during run-up, which yielded the time-constant indicated above. (**F**) Comparison of the run-up duration observed with Ba^{2+} or Ca^{2+} as the charge carrier (same cells as in E). **(G)** Mean current traces evoked by a 50-ms voltage ramp from −80 mV to 60 mV immediately after establishing the whole-cell configuration (I_{start}, blue solid line), at the time of maximum I_{Ba} (I_{max}, black solid line) and after 7 min of run-down (I_{7min}, orange broken line; *n* = 7). Inset: Same current traces but scaled to their maximum value to illustrate the lack of changes in position and shape during run-up and subsequent left shift of the curve during run-down. **, P < 0.01; ***, P < 0.001 vs. Ctrl in B and C or vs. Ba^{2+} in F (one-way ANOVA with Bonferroni post-hoc correction). Values are expressed as mean ± SEM.

changes in $Ca_v2.3$ channel current were still observed when recordings were performed under static (i.e., without perfusion) conditions (*n* = 3; not depicted). As would be expected for a process that involves diffusion-controlled depletion of metabolic substrates or other cytosolic factors on the other hand, the time course but not magnitude of changes in I_{Ba} depended on the absolute values of R_s (i.e., cell–pipette coupling) and C_s (i.e., cell size), so that combined use of smaller pipette tip diameters (R_s = 12 ± 1 MΩ) and larger cells (C_s = 29 ± 6 pF) resulted in a significant slowing of run-up and run-down compared with standard recording conditions (Fig. 2, A–D). Unless noted otherwise, the following experiments were all performed under standard recording conditions to facilitate fast and reproducible cell dialysis.

As shown in Fig. 2 E, the characteristic sequence of changes was also observed when recordings were performed with 5 mM Ca^{2+} as the charge carrier (Fig. 2 E), although run-up was significantly faster (Fig. 2 F) and appeared to be more complete when compared with parallel recordings with 5 mM Ba^{2+}. Moreover, I_{start} (but not I_{max} or I_{7min}) was significantly larger in recordings performed with Ca^{2+}, suggesting that run-up but not run-down may be initiated or facilitated by a Ca^{2+}-dependent mechanism.

Because changes in the ionic conditions during cell dialysis could affect currents by altering the driving force, we also examined the quasi-steady-state voltage dependence of I_{Ba} with a 50-ms voltage-ramp from −80 to 60 mV (Fig. 2 G). Run-up was similar over the whole voltage range and not associated with changes in the apparent reversal potential (V_{rev}), so that initial (I_{start}, blue solid line) and run-up (I_{max}, black solid line) currents overlapped almost completely when scaled to their maximum amplitude (Fig. 2 G, inset). Currents recorded after partial run-down (I_{7min}, orange dotted line) still had the same V_{rev}, but were shifted to more negative stimulus voltages, suggesting that their decline is not the result of a change in driving force but influenced by the test potential.

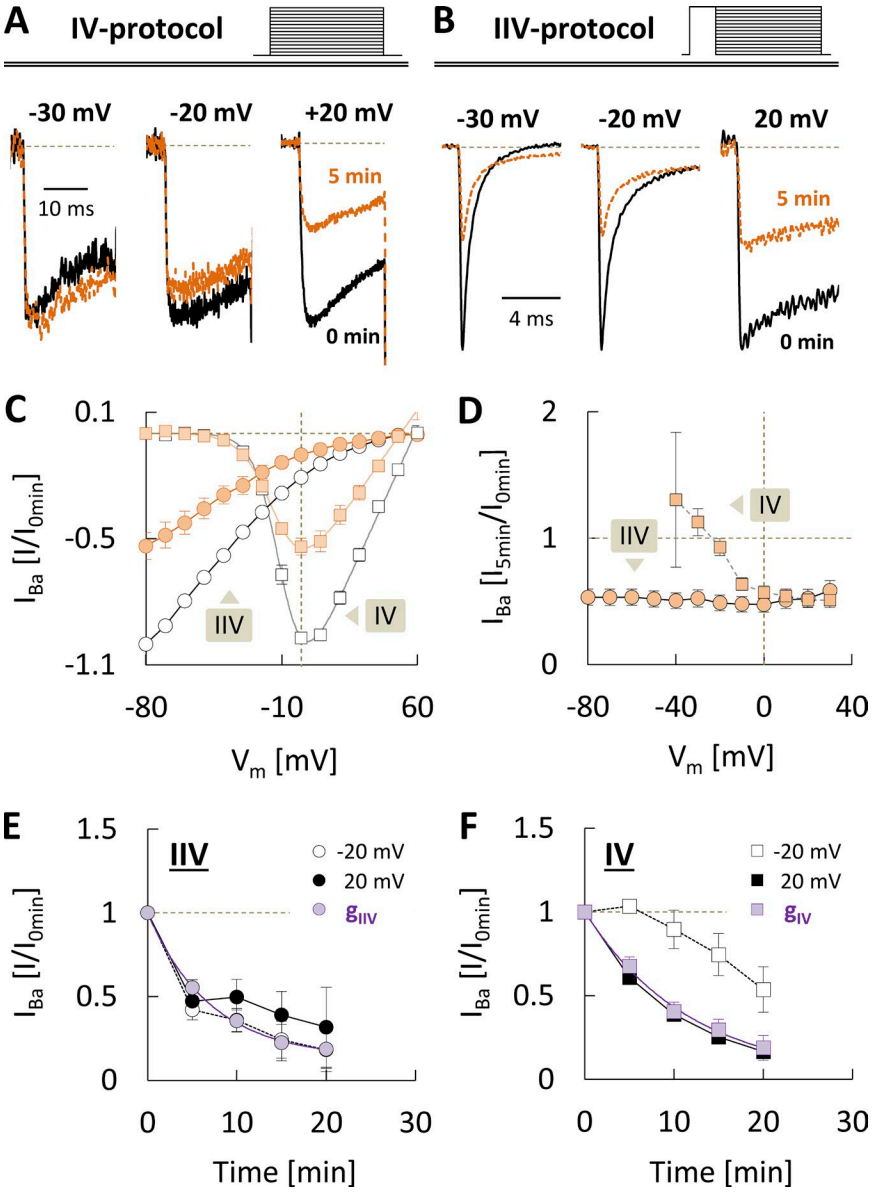

Figure 3. **Voltage dependence of steady-state and instantaneous current decline. (A)** Mean steady-state (IV) currents (n = 6) recorded at the indicated test potentials before (black lines) and after 5 min of run-down (orange lines). To allow for comparison of the relative change at different test potentials, they have been normalized to the peak current amplitude observed at each voltage before run-down. **(B)** Mean instantaneous (IIV) currents recorded from the same cells as in A before (black lines) and after 5 min of run-down (orange lines). To allow for comparison of the relative change at different test potentials, they have been normalized as in A. **(C)** Comparison of steady-state IV (squares) and IIV (circles) relationships, determined immediately after complete run-up (open symbols) and after 5 min of run-down (orange symbols; same cells as in A and B). **(D)** Voltage dependence of the fraction of IV (squares) and IIV (circles) current remaining after 5 min of run-down, determined as the ratio between current amplitudes after 5 min of run-down and current amplitudes at time 0 (same cells as in A–C). **(E)** Mean changes over time in the fraction of IIV current recorded at −20 mV (open circles with dotted line) and +20 mV (black circles with solid line) and in the slope conductance (g_{IIV}) between −80 and 0 mV (same cells as in A–D). **(F)** Mean changes over time in the fraction of IV current recorded at −20 mV (open squares with dotted line) and +20 mV (black squares with solid line) and in the maximum slope conductance (g_{IV}) determined from IV relationships (same cells as in A–E). Values are expressed as mean ± SEM.

Run-down involves separable changes in gating and maximum conductance

The macroscopic conductance of a uniform population of voltage-gated channels can be approximated by the product of (1) the voltage- and time-dependent channel open probability (P_O), (2) the holding potential-dependent availability for activation (P_F), and (3) the voltage-independent maximum macroscopic conductance (G_{max}), which depends on single-channel conductance (γ), the total number of channels (N), and the maximum values of P_O ($P_{O,max}$) and P_F ($P_{F,max}$). In this framework, run-down could involve reduced activation, increased inactivation, and/or an intrinsically voltage-dependent decrease of G_{max}. In a first attempt to distinguish between these possibilities, we compared steady-state (IV) and instantaneous (IIV) current-voltage relationships, determined at the onset of run-down and in 5-min intervals thereafter (Fig. 3, A–C). Because IIV currents were recorded immediately after a brief prepulse to open most channels available for activation, they should be little affected by changes in the voltage-dependence of P_o. Fig. 3 D plots the fraction of IV and IIV currents that remained after partial run-down for 5 min as a function of the test potential. The decline of steady-state currents increased with voltage but reached voltage-independent values at positive test potentials (where P_O approaches $P_{O,max}$), which is consistent with the shift of ramp-evoked currents (Fig. 2 G). When measured with the IIV protocol on the other hand, run-down was about the same at different test potentials and similar to IV-current decline at depolarized voltages (Fig. 3 D). The same pattern was observed at the later time points examined, so that the kinetics of IIV-current run-down were well represented by the exponential decline in slope conductance between −80 and 0 mV (τ = 7 ± 2 min, g_{IIV} in Fig. 3 E). The time course of IV-current decline was markedly delayed during weak depolarization but similar when it was measured at sufficiently positive test potentials (τ = 9 ± 1 min) or in terms of the maximum slope conductance (τ = 10 ± 2 min,

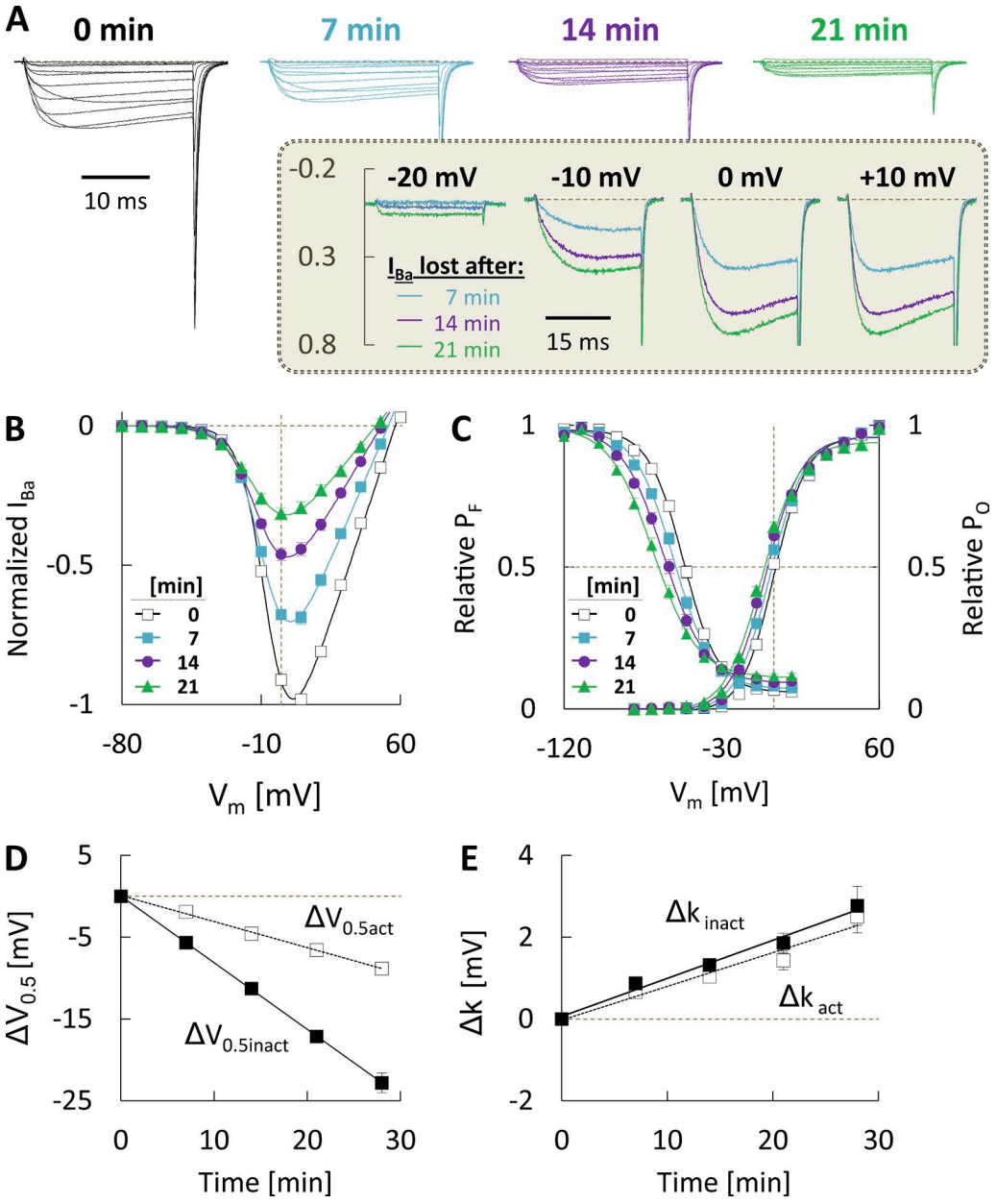

Figure 4. **Changes in channel voltage dependence during run-down. (A)** Families of mean IV currents (n = 8) evoked by 25 ms voltage steps to test potentials between −80 mV and +60 mV at the onset of run-down (0 min) and in 7-min intervals thereafter. They have been normalized to the maximum peak I_{Ba} at time 0. Inset: Current lost to run-down at the indicated test potentials, determined by subtracting from the normalized current traces recorded at time 0 the corresponding traces recorded after 7 (orange lines), 14 (purple lines), and 21 min (green lines) of run-down. **(B)** Mean IV relationships measured at the same time points as in A and normalized to the maximum peak current amplitude recorded at time 0 (n = 49). **(C)** Voltage dependence of activation (right) and prepulse inactivation (left), determined at the same time points as in A (same cells as in B). **(D)** Time course of changes in the half-activation ($V_{0.5act}$) and half-inactivation ($V_{0.5inact}$) voltages, determined from single Boltzmann fits to the data in C. **(E)** Time course of changes in the activation (k_{act}) and inactivation (k_{inact}) slope factors, determined from single Boltzmann fits to the data in C. Values are expressed as mean ± SEM.

g_{IV} in Fig. 3 F). Based on these findings, the decrease of macroscopic conductance by itself was independent of the test-pulse potential and had an approximately exponential time course, so the apparent voltage-dependence must have derived from changes in the voltage dependence of P_O, which (partly) counteracted IV-current decline and even caused some transient stimulation at negative test potentials.

Run-down is paralleled by changes in channel voltage dependence

To assess how changes in the voltage dependence of P_O and P_F are involved in current decline, we compared IV, activation, and prepulse inactivation curves (for details on the voltage protocols see Materials and methods), determined at different time points after the onset of run-down. Fig. 4 summarizes the results

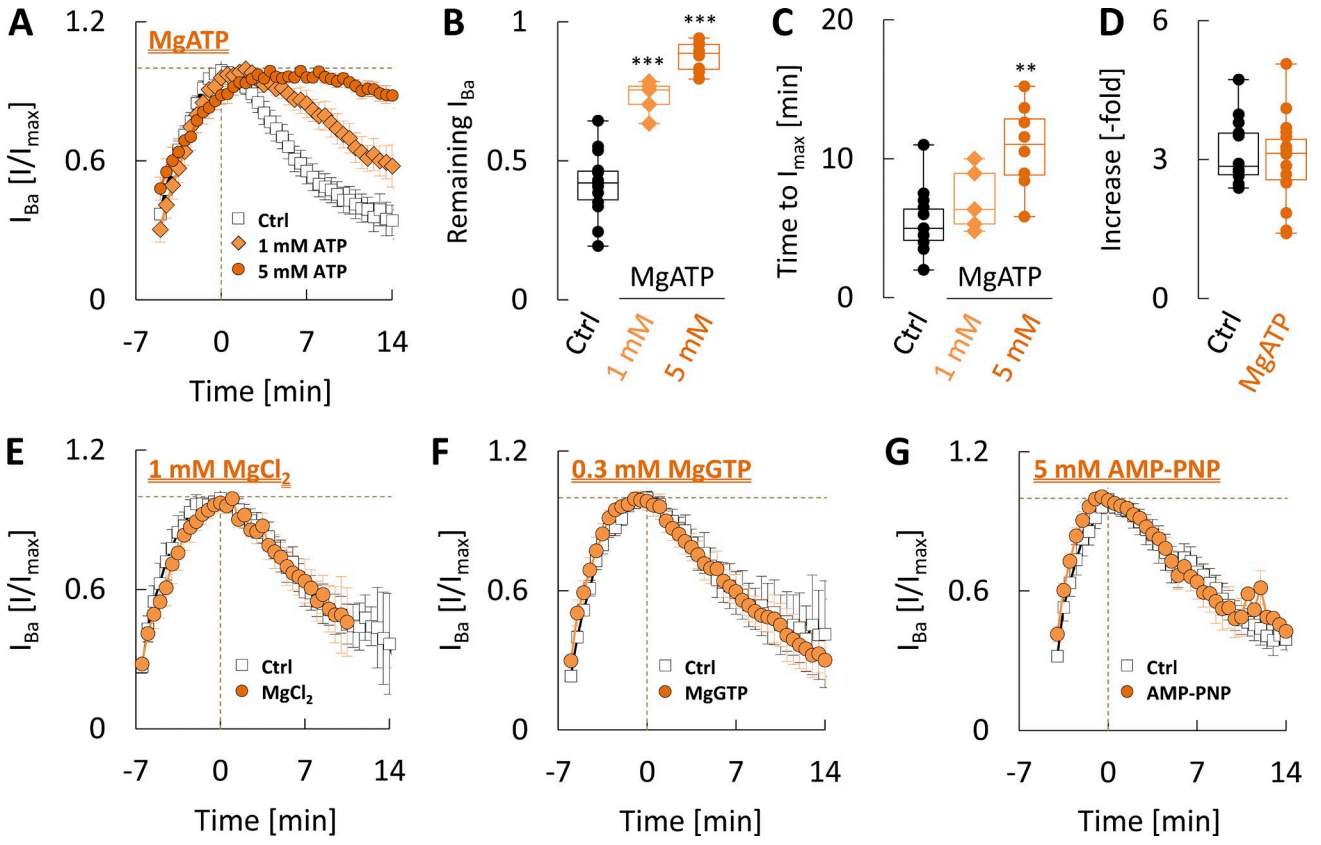

Figure 5. **Hydrolysable ATP provides protection from $Ca_v2.3$ channel run-down.** Comparison between time-course recordings performed with the indicated test substances and parallel control recordings with standard internal solution. **(A)** Mean data from 5 recordings with 1 mM MgATP (orange squares), 8 recordings with 5 mM MgATP (orange circles), and 13 parallel control recordings (open squares). **(B)** Comparison of the residual I_{Ba} after 7 min of run-down under control conditions and with 1 or 5 mM MgATP in the pipette solution (same cells as in A). **(C)** Comparison of the run-up duration under control conditions and with 1 or 5 mM MgATP in the pipette solution (same cells as in A). **(D)** Comparison of the current increase under control conditions and with 1–5 mM MgATP in the pipette solution (same cells as in A). **(E)** Mean data from five recordings with 1 mM $MgCl_2$ (orange squares) and seven parallel control recordings (open squares). **(F)** Mean data from six recordings with 0.3 mM MgGTP (orange squares) and five parallel control recordings (open squares). **(G)** Mean data from eight recordings with 5 mM AMP-PNP (orange squares) and seven parallel control recordings (open squares). **, $P < 0.01$; ***, $P < 0.001$ vs. Ctrl (one-way ANOVA with Bonferroni post hoc correction). Values are expressed as mean ± SEM.

obtained in a total of 49 cells (C_{slow} = 29 ± 2 pF), from which meaningful currents could be recorded for at least 21 min. The shape of IV current lost to run-down (Fig. 4 A, inset), was essentially identical to the shape at time 0 and contained a prominent ON-gating current component, suggesting that run-down reduced the total number of active channels (i.e., P_F at −80 mV, $P_{F,max}$, and/or N). It was paralleled by progressive but unequal hyperpolarizing shifts of activation and prepulse inactivation, which are illustrated in Fig. 4 (C and D). The half-activation voltage ($V_{0.5act}$) significantly decreased from 0 ± 1 mV at time 0 to −6 ± 1 mV ($P < 0.001$) after 21 min of run-down, corresponding to a shift by roughly −6 mV. In the same time, the half-inactivation voltage ($V_{0.5inact}$) significantly decreased from −52 ± 1 mV to −69 ± 1 mV ($P < 0.001$), corresponding to a shift by roughly −17 mV. In both cases, the rate of shift in individual recordings could be well described by linear fits to the changes in half-point as a function of time, with slopes of −0.33 ± 0.02 mV/min (adjusted R^2 = 0.90 ± 0.02) for activation and −0.82 ± 0.03 mV/min (adjusted R^2 = 0.95 ± 0.01) for inactivation. Based on these findings, P_F at −80 mV was reduced by ∼5, 12, and 19% after 7, 14, and 21 min of run-down, respectively (Fig. 4 C), which corresponds to a constant rate of roughly 1%/min. In the same time, g_{IV} declined by ∼25, 47, and 61%, so that reduced availability for activation alone could only explain part of the IV-current decline at positive test potentials (Fig. 4 B). Together with a complete loss of gating currents during run-down, these findings suggested that the decline in conductance involves additional (holding potential–independent) changes in the number of active channels (i.e., N and/or $P_{F,max}$). This was also evident in time-course recordings where the holding potential after partial run-down was made more negative, which led to considerable but incomplete recovery of the current at 10 mV (not depicted).

In addition to the shift, run-down reduced the steepness of both curves in Fig. 4 C, which was reflected in a gradual increase of the activation and inactivation slope factors (k_{act} and k_{inact}) from 9.0 ± 0.2 and 9.2 ± 0.1 mV/e-fold change at time 0 to 10.5 ± 0.3 ($P < 0.001$) and 11.1 ± 0.3 ($P < 0.001$) mV/e-fold change after 21 min of run-down, respectively (Fig. 4 E).

Hydrolysable ATP provides protection from run-down

Because one of the most common reasons for "washout" of ionic currents is a decrease in the level of intracellular high-energy

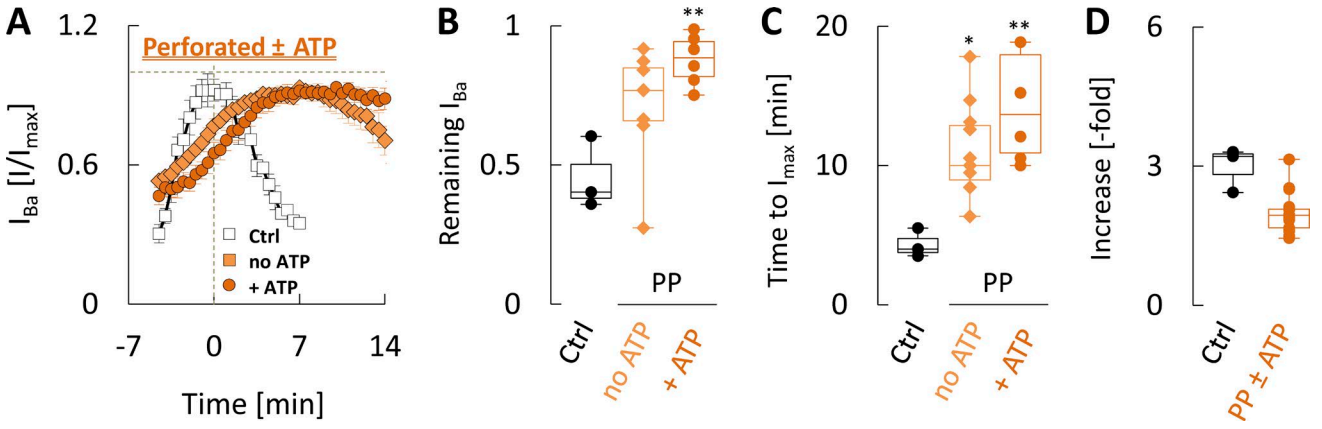

Figure 6. **ATP protection from run-down is reproduced by perforated-patch recordings.** Comparison of time-course recordings with 40 µM β-escin in the absence and presence of MgATP. **(A)** Mean data from 11 perforated-patch recordings with standard internal solution (orange diamonds), 6 perforated-patch recordings with 5 mM MgATP (orange circles), and 3 perforated-patch recordings with standard internal solution in which the patch ruptured during perforation (open squares). All recordings were performed with 40 µM β-escin as the perforating agent. **(B)** Comparison of the residual I_{Ba} after 7 min of run-down in recordings with patch rupture and in perforated recordings without or with 5 mM MgATP (same cells as in A). **(C)** Comparison of the run-up duration in recordings with patch rupture and in perforated recordings without or with 5 mM MgATP (same cells as in A). **(D)** Comparison of the current increase in recordings with patch rupture and in perforated recordings without or with 5 mM MgATP (same cells as in A). *, $P < 0.05$; **, $P < 0.01$ vs. Ctrl (one-way ANOVA with Bonferroni post hoc correction). Values are expressed as mean ± SEM.

compounds or other cytosolic factors, we next tested if different forms and concentrations of nucleotide triphosphates, a cytosolic extract, and/or perforated-patch recordings are effective in altering run-down. To this end, the time course of changes in peak I_{Ba} under various experimental conditions was quantified as described above and compared with parallel control recordings performed with standard internal solution (Figs. 5 and 6). To facilitate comparison of effects between the different experiments, Fig. 7 summarizes mean changes expressed relative to the corresponding control recordings (i.e., Δ Increase, Δ Time to I_{max}, and Δ Remaining I_{Ba}), which were determined by subtracting from each individual value with the indicated test solutions the mean value determined in parallel control recordings (for details see Materials and methods). As can be seen in Fig. 5, addition of 1–5 mM MgATP to the pipette solution significantly increased the current fraction that remained after 7 min of run-down compared with parallel control recordings (Fig. 5, A and B) and produced a concentration-dependent slowing of run-up (Fig. 5, A and C). These effects were not attributable to changes in intracellular free Mg^{2+} (~0.4 mM with 5 mM MgATP) because addition of 1 mM $MgCl_2$ alone (~0.5 mM free Mg^{2+}) to the standard internal solution affected neither run-up nor run-down (Fig. 5 E). Moreover, with a pipette solution containing 5 mM NaATP and no added free Mg^{2+}, there was still a significant slowing of run-up and a significant increase of the current fraction remaining after 7 min of run-down (Fig. 7, A and C).

ATP protection from run-down was about the same with different charge carriers (i.e., Ba^{2+} vs. Ca^{2+}) and not altered when the nucleotide was combined with 3 µM CaM (Fig. 7 C). Supplementation of the pipette solution with 0.3 mM MgGTP (Fig. 5 F) or 5 mM of the nonhydrolyzable ATP-analogue AMP-PNP (Fig. 5 G) on the other hand affected neither run-up nor run-down (Fig. 7). Together, these findings argue against a role of direct nucleotide binding and indicate a requirement for ATP-hydrolysis and transfer of the phosphate group.

Note also that (with Ba^{2+} as the charge carrier) none of the manipulations tested significantly altered the magnitude of run-up (Figs. 5 B and 7 B) or the absolute values of I_{max} (not depicted), suggesting that ATP can slow but not prevent the processes underlying run-up. The apparent increase in the magnitude of run-up by ATP observed with Ca^{2+} as the charge carrier (Fig. 7 B) was also not related to a more pronounced up-regulation of I_{Ca} per se because absolute values of I_{max} were the same as in parallel control recordings (not depicted). Although there was a tendency for I_{start} to be smaller in recordings with ATP, this effect could hardly be ascribed to an action of the nucleotide. Because the faster run-up kinetics in Ca^{2+} hampered accurate determination of I_{start}, it might instead have resulted from small differences between groups in the time required for R_s to stabilize after patch-rupture.

ATP protection is reproduced by perforated-patch recordings

In principle, exogenous ATP might counteract run-down by preventing a decrease of cytosolic nucleotide levels or by increasing them above the normal value in intact cells, thereby stimulating the channels through an unrelated mechanism. To distinguish between these two possibilities, we performed perforated-patch recordings with β-escin, diluted into the same internal recording solution as in ruptured-patch experiments. ATP-diffusion through β-escin pores has been demonstrated, but perforating efficiency is concentration and time dependent, so washout should be considerably slower than in ruptured-patch recordings (Arnould et al., 1996; Fan and Palade, 1998; Fu et al., 2003). As illustrated in Fig. 6 A and summarized in Fig. 7, the time course of changes during perforated recordings was very similar to that observed in ruptured recordings with ATP. Importantly, and consistent with a role of ATP-depletion for the current decline, perforated recordings were almost as effective in reducing run-down as provision of ATP in ruptured recordings. Moreover, the protective

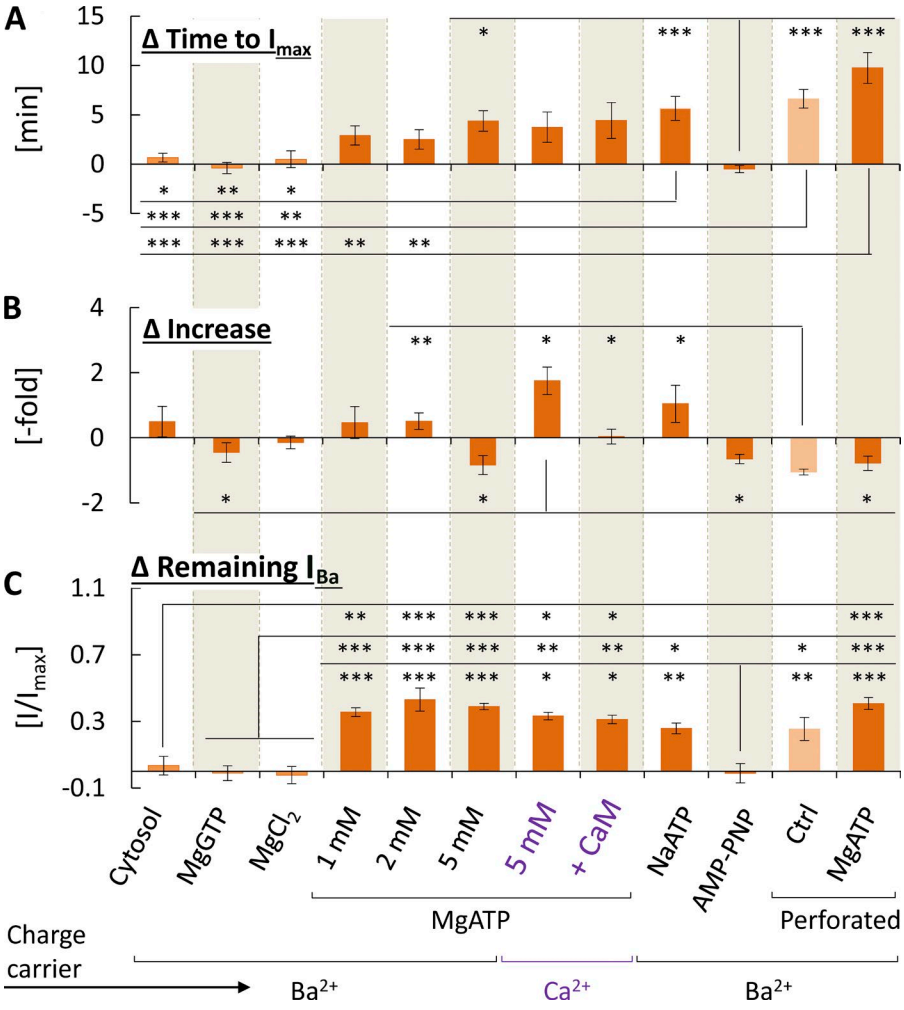

Figure 7. **Overview of changes in run-up and run-down observed under various experimental conditions.** Data are from the same cells as in Figs. 5 and 6 with additional data from 7 recordings with cytosolic extract (Cytosol) and 6 parallel control recordings, 9 recordings with 5 mM NaATP and 7 parallel control recordings, and 13 recordings performed with Ca^{2+} as the charge carrier and 5 mM MgATP in the presence or absence of 3 µM CaM plus 5 parallel control recordings. For comparison between the different experimental conditions, all values obtained with a given test solution were normalized by subtracting the mean value observed in parallel control recordings and then averaged, so the derived parameters provide a measure for the mean change relative to control (for details see Materials and methods). Symbols for statistical significance refer to the comparison of normalized values between different experimental conditions. **(A)** Comparison of mean changes relative to parallel control recordings in the duration of run-up (Δ Time to I_{max}). **(B)** Comparison of mean changes relative to parallel control recordings in the magnitude of run-up (Δ Increase). **(C)** Comparison of mean changes relative to parallel control recordings in the residual current after 7 min of run-down (Δ Remaining I_{Ba}). *, $P < 0.05$; **, $P < 0.01$; ***, $P < 0.001$ (one-way ANOVA with Bonferroni post hoc correction in A and C or Welch's ANOVA with the Games-Howell multiple-comparison method in B). Values are expressed as mean ± SEM.

effects of perforated recordings and ATP were not additive, so that provision of 5 mM MgATP in perforated recordings produced the same effects as in ruptured recordings (Figs. 6 B and 7 C). Collectively, these findings indicate that both, perforated recording and/or provision of ATP reduced run-down by preventing depletion of the nucleotide during the recordings. This is in contrast to the effects on run-up duration, which were much more pronounced in perforated recordings and further increased in the presence of ATP (Figs. 6 C and 7 A). Moreover, because our measurements were started only after R_s had reached values ≤15 MΩ, we most likely missed part of the run-up process, so these results may still underestimate the true slowing of run-up in perforated recordings. Thus, the initial but not maximum peak current density was significantly larger in perforated recordings (not depicted), and this was reflected in a reduced magnitude of run-up (Figs. 6 D and 7 B). Together, these observations point to the involvement of additional cytosolic factors during run-up, which are more effectively retained in perforated-patch recordings. However, a cytosolic extract prepared in standard internal solution (4.32 mg protein/ml) was ineffective in altering run-up or run-down (Fig. 7), possibly because these factors depend on the additional presence of ATP.

ATP stabilizes channel gating and maximum conductance

All the above findings supported the assumption that $Ca_v2.3$ channel run-down and, to some extent, run-up in dialyzed cells are related to a depletion of cytosolic ATP. Because it was of interest how ATP affects the different alterations associated with run-down, we reexamined the changes in channel voltage dependence during current decline with a pipette solution supplemented with 5 mM MgATP. As illustrated in Fig. 8 A, inclusion of ATP completely abolished the early phase of current decline, so that on average, g_{IV} after 7 min of run-down amounted to 97 ± 7% of its initial value ($n = 6$). In addition, the stabilizing action of ATP was associated with an almost complete prevention of time-dependent changes in channel voltage dependence and sensitivity (Fig. 8, B–E), suggesting that basal ATP-dependent modulation alters channel-gating behavior and is required for maintaining it in a functional state.

The effects of ATP are not related to lipid kinase–mediated PIP_2 synthesis

Because run-down of several neuronal VGCCs and its reversal by MgATP have been linked to depletion and resynthesis of membrane PIP_2, respectively (Wu et al., 2002; Suh et al., 2010), we next examined the effects of wortmannin (WM), a potent and

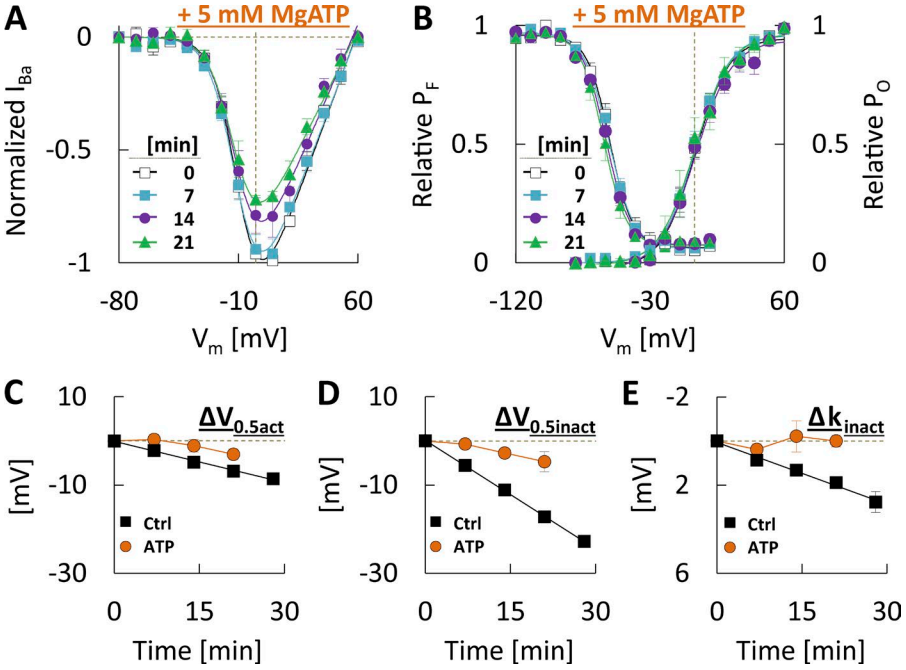

Figure 8. **Hydrolysable ATP stabilizes $Ca_v2.3$ channel gating and function. (A)** Mean IV relationships measured at the onset of run-down and in 7-min intervals thereafter with a pipette solution containing 5 mM MgATP (n = 6). **(B)** Voltage dependence of activation (right) and prepulse inactivation (left), determined at the same time points as in A (same cells as in A). **(C)** Time course of changes in the half-activation voltage during run-down observed in the absence (black squares, same cells as in Fig. 4) and presence (orange circles, same cells as in A) of 5 mM MgATP. **(D)** Time course of changes in the half-inactivation voltage during run-down observed in the absence (black squares, same cells as in Fig. 4) and presence (orange circles, same cells as in A) of 5 mM MgATP. **(E)** Time course of changes in the inactivation slope factor during run-down observed in the absence (black squares, same cells as in Fig. 4) and presence (orange circles, same cells as in A) of 5 mM MgATP. Values are expressed as mean ± SEM.

irreversible lipid kinase inhibitor (Wipf and Halter, 2005). When MgATP in the pipette solution was combined with 10 µM WM (ATP+WM in Fig. 9, A–D), it still significantly increased the current fraction remaining after 7 min of run-down (Fig. 9 B) and markedly slowed run-up (Fig. 9 C). Relative to recordings with MgATP alone, WM actually tended to enhance the protective effects (Fig. 10 C), suggesting that it increased ATP availability because of reduced consumption by lipid kinases. Likewise, pretreatment of cells by incubation in extracellular solution containing 10 µM WM for 15 min (ATP+WM PT in Fig. 9, A–D) did not significantly impair the stabilizing action of MgATP (Fig. 9 B) nor did it alter the time course of changes observed in parallel control recordings. Unlike acute treatment (i.e., ATP+WM) however, WM pretreatment markedly enhanced the ATP-induced slowing of run-up in a subset of cells (Fig. 9 C), so that on average, the latter effect was stronger but also more variable (Fig. 10 A). A similar modification of ATP-induced changes in the duration of run-up was observed in only one of seven recordings with ATP+WM (Fig. 9 C), suggesting that PIP_2 depletion rather than acute inhibition of its resynthesis may be required to modify ATP-effects on run-up. Brief application of WM inhibits PIP_2 replenishment without affecting PIP_2 hydrolysis (Zhang et al., 2003), so the variable effectiveness of WM pretreatment might have been related to differences in lipid turnover and degree of actual PIP_2 depletion between cells. Regardless of the exact effects on run-up however, the protection by ATP against run-down was clearly unaffected by WM, suggesting that it was not related to lipid kinase–mediated mechanisms and arguing against a role of PIP_2 depletion for $Ca_v2.3$ channel run-down in our system.

Another line of reasoning has been that not PIP_2 depletion itself, but rather accumulation of one of its fatty acid cleavage products, arachidonic acid (AA), is responsible for run-down of some neuronal VGCCs (Liu et al., 2001, 2006; Liu and Rittenhouse, 2003). However, neither 1 mg/ml of the AA-scavenger BSA (Fig. 9 E) nor 5 µM of the phospholipase C inhibitor U73122 (Fig. 9 F) affected the time course of run-up or run-down when they were added to the (ATP-free) internal solution (Fig. 10, A–C).

The effects of ATP depend on protein kinase–mediated phosphorylation

We next examined the role of changes in protein phosphorylation and dephosphorylation, which may result from ATP-depletion and have been implicated in the run-down of L-type high-voltage-activated Ca^{2+} channels (Armstrong and Eckert, 1987; Hilgemann, 1997). As summarized in Fig. 10 (A–C), the effects of MgATP were well preserved and again even somewhat enhanced when it was combined with 100 µM of the protein tyrosine kinase inhibitor genistein (GS). Combination with 10 µM of the broad-spectrum serine/threonine kinase inhibitor stauro on the other hand completely abolished MgATP effects on the duration of run-up, so the time to I_{max} with MgATP+stauro was not significantly different from the time course in parallel control recordings (Fig. 11, A–C; and Fig. 10 A). Moreover, although MgATP in the presence of stauro still significantly increased the fraction of current remaining after 7 min of run-down relative to parallel control recordings (Fig. 11, A and B), the net effect was significantly reduced when compared with that observed in other recordings with MgATP. Thus, expressed relative to the corresponding control recordings, MgATP+stauro was significantly less effective in increasing the current fraction after 7 min of run-down than MgATP alone, MgATP+WM, or MgATP+GS (Fig. 10 C).

There was no evident effect of stauro in the absence of ATP (Fig. 11, A–C), indicating that it acted by reducing ATP-protection from run-down. From these findings it follows that the ATP-induced slowing of run-up and most but not all the protection from run-down must have involved protein kinase–mediated phosphorylation of serine/threonine residues. On the other hand, run-down in the absence of ATP might reflect a progressive

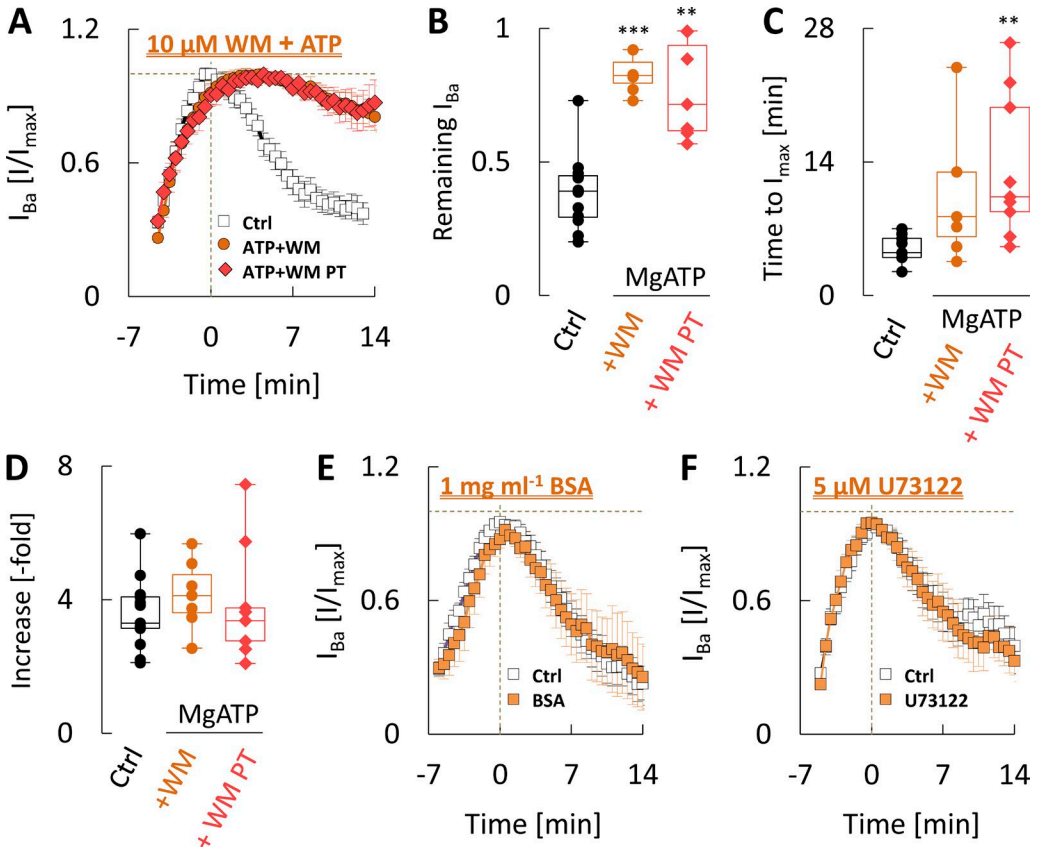

Figure 9. **ATP protection from run-down is not related to increased PIP_2 synthesis. (A)** Mean data from seven recordings with 5 mM MgATP and 10 µM WM (ATP + WM), nine recordings with 5 mM MgATP after WM pretreatment (ATP + WM PT), and 13 parallel control recordings. **(B)** Comparison of the residual I_{Ba} after 7 min of run-down under control conditions, with ATP and WM and with ATP after WM pretreatment (same cells as in A). **(C)** Comparison of the run-up duration under control conditions, with ATP and WM and with ATP after WM pretreatment (same cells as in A). **(D)** Comparison of the current increase under control conditions, with ATP and WM and with ATP after WM pretreatment (same cells as in A). **(E)** Mean data from five recordings with 1 mg/ml BSA and nine parallel control recordings. **(F)** Mean data from six recordings with 5 µM U73122 and eight parallel control recordings. **, P < 0.01; ***, P < 0.001 vs. Ctrl (one-way ANOVA with Bonferroni post hoc correction). Values are expressed as mean ± SEM.

decrease of channel phosphorylation because of changes in the balance between constitutive de- and rephosphorylation. To test this assumption, we examined the effects of a sustained (30–60-min) incubation of cells in extracellular solution containing 1 µM stauro, which should mimic run-down by reducing basal protein phosphorylation. Consistent with (partial) run-down of the channels before establishment of the recordings, stauro pretreatment increased the number of cells lacking macroscopic currents and significantly reduced both I_{start} and I_{max} in the remaining cells (Fig. 11, D–F). Interestingly, it also significantly increased the magnitude and duration of run-up (Fig. 11, G–I), although the latter effect may have been related to the appearance of a plateau phase with little change in current amplitudes for several minutes. Subsequently, run-down proceeded with a normal time course, so the decrease of currents after 7 min was essentially the same as in parallel control recordings.

To assess how these effects were related to the ATP-sensitive gating changes, we also examined the effects of stauro pretreatment on channel voltage dependence (Fig. 12). As illustrated in Fig. 12 (B and C), activation and prepulse inactivation curves recorded in pretreated cells before the onset of run-down showed a significant shift to more negative test potentials when compared with the results obtained in untreated cells, although the voltage-sensitivity (i.e., k_{act} and k_{inact}) was similar (not depicted).

In addition, stauro pretreatment tended to accelerate the voltage shifts during run-down (Fig. 12, D and E), although comparison of the exact time course is confounded by differences in cell size between the experiments, so no firm conclusions can be drawn from this finding. Interestingly however, it also effectively prevented the decrease in activation voltage sensitivity during run-down (Fig. 12 F) without altering the changes in inactivation voltage sensitivity (not depicted), possibly pointing to the involvement of multiple mechanisms at distinct sites.

Because the serine/threonine phosphatase calcineurin has been shown to interact with neuronal VGCCs (Chad and Eckert, 1986; Fomina and Levitan, 1997) and implicated in the run-down of certain K^+ channels (Horváth et al., 2002), we also tested the effects of pretreating cells with a 60-min incubation in extracellular solution containing 10 µM of the membrane-permeable calcineurin-inhibitor deltamethrin (DM). However, the time course of changes in I_{Ba} observed in DM-pretreated cells (recorded with ATP-free pipette solution) was not significantly different from that in parallel control recordings (Fig. 10).

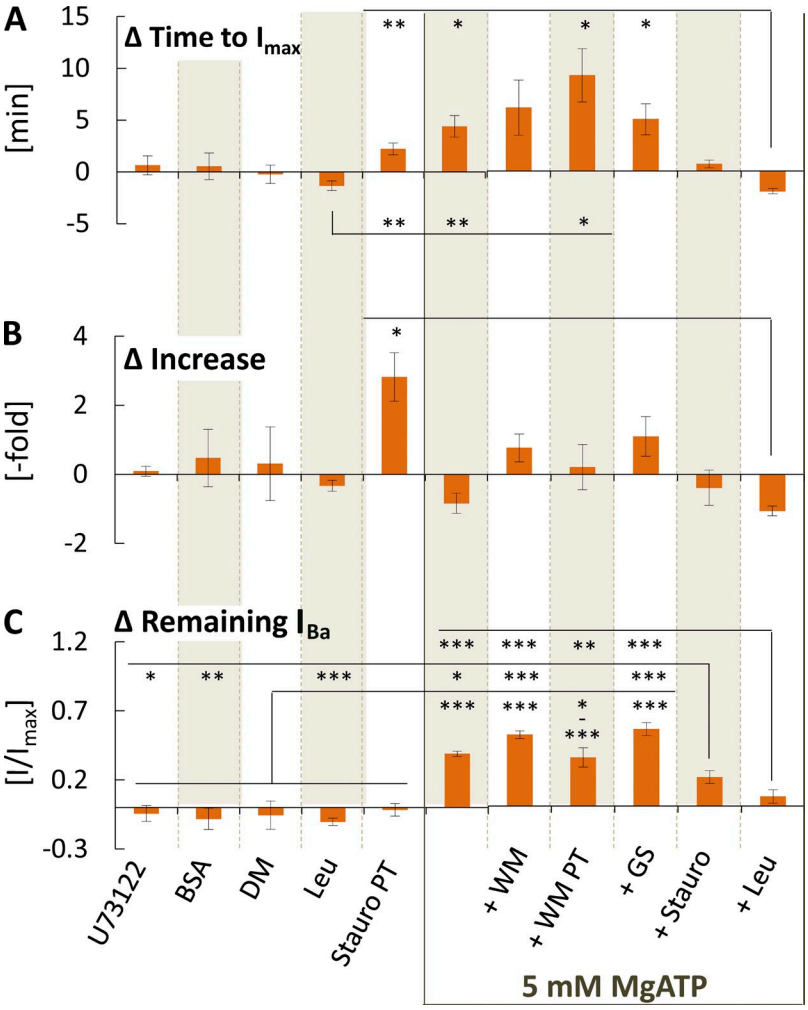

Figure 10. **Overview of changes in run-up and run-down observed under various experimental conditions.** Data are from the same cells as in Figs. 9, 11, and 13 with additional data from six recordings with 5 mM MgATP + 100 µM GS (+GS) and four parallel control recordings and three recordings after a 60-min pretreatment with 10 µM DM and five parallel control recordings. For comparison between the different experimental conditions, all values obtained with a given test solution were normalized as described in Fig. 7 and Materials and methods. Symbols for statistical significance refer to the comparison of normalized values between different experimental conditions. **(A)** Comparison of mean changes relative to parallel control recordings in the duration of run-up (Δ Time to I_{max}). **(B)** Comparison of mean changes relative to parallel control recordings in the magnitude of run-up (Δ Increase). **(C)** Comparison of mean changes relative to parallel control recordings in the residual current after 7 min of run-down (Δ Remaining I_{Ba}). *, $P < 0.05$; **, $P < 0.01$; ***, $P < 0.001$ (one-way ANOVA with Bonferroni post hoc correction in A and C or Welch's ANOVA with the Games-Howell multiple-comparison method in B). Values are expressed as mean ± SEM.

Run-up may involve activation of Leu-sensitive proteases

Finally, we performed experiments with Leu, a protease inhibitor that has been shown to prevent an irreversible ATP-resistant component of run-down in L-type VGCCs (Chad and Eckert, 1986; Elhamdani et al., 1994). Unexpectedly, and in contrast to all other manipulations tested, MgATP+100 µM Leu significantly decreased the magnitude of run-up (Fig. 13, A–C), so that I_{start} was similar but I_{max} was approximately half of the value observed in parallel control recordings. In addition, Leu not only abolished the MgATP-dependent slowing of run-up but actually produced a significant decrease of the time to I_{max} when it was combined with ATP (Fig. 13 D). Apart from altering the time course and net increase of currents, ATP+Leu reduced cell-to-cell variability in the magnitude of run-up (variance = 0.89 in control recordings vs. 0.16 with MgATP+Leu, $P < 0.05$) and diminished the initial slowing of inactivation (Fig. 13 C), indicating that both processes may be related to activation of Leu-sensitive proteases and influenced by variable endogenous protease and/or protease inhibitor levels.

Curiously, Leu also suppressed the protective effect of MgATP against run-down (Fig. 13 A), so that expressed relative to the corresponding control recordings, MgATP+Leu was significantly less effective against rundown than MgATP alone, MgATP+WM, MgATP after WM pretreatment, or MgATP+GS (Fig. 10 C). When the same concentration of Leu (100 µM) was used in the absence of MgATP, it had similar but quantitatively much less marked effects on run-up (Fig. 13, A–D) and no effect on the degree of run-down (Fig. 10 C) or the inactivation changes during run-up (Fig. 13 E).

Discussion

In the present study, we used conventional and perforated-patch-clamp recordings in a recombinant expression system to assess changes in $Ca_v2.3$ channel currents during cell dialysis. Our findings recapitulate studies about their native counterparts and show that dialysis with ATP-free internal solutions produces a characteristic sequence of run-up and run-down, the time-course of which depends on R_s, cell size, and recording configuration. The exponential decline in conductance during run-down by itself was voltage independent but paralleled by a progressive shift of channel voltage dependence to more negative test potentials. The voltage-shift reduced channel availability at the holding potential (i.e., P_F) but proceeded at a constant rate and could only partly account for the complete loss of gating currents during run-down. Therefore, most of the decline in conductance was related to changes in the total number of functional channels (i.e., N and/or $P_{F,max}$) and possibly to other factors (i.e., decrease of γ or $P_{O,max}$). Run-down and all the associated

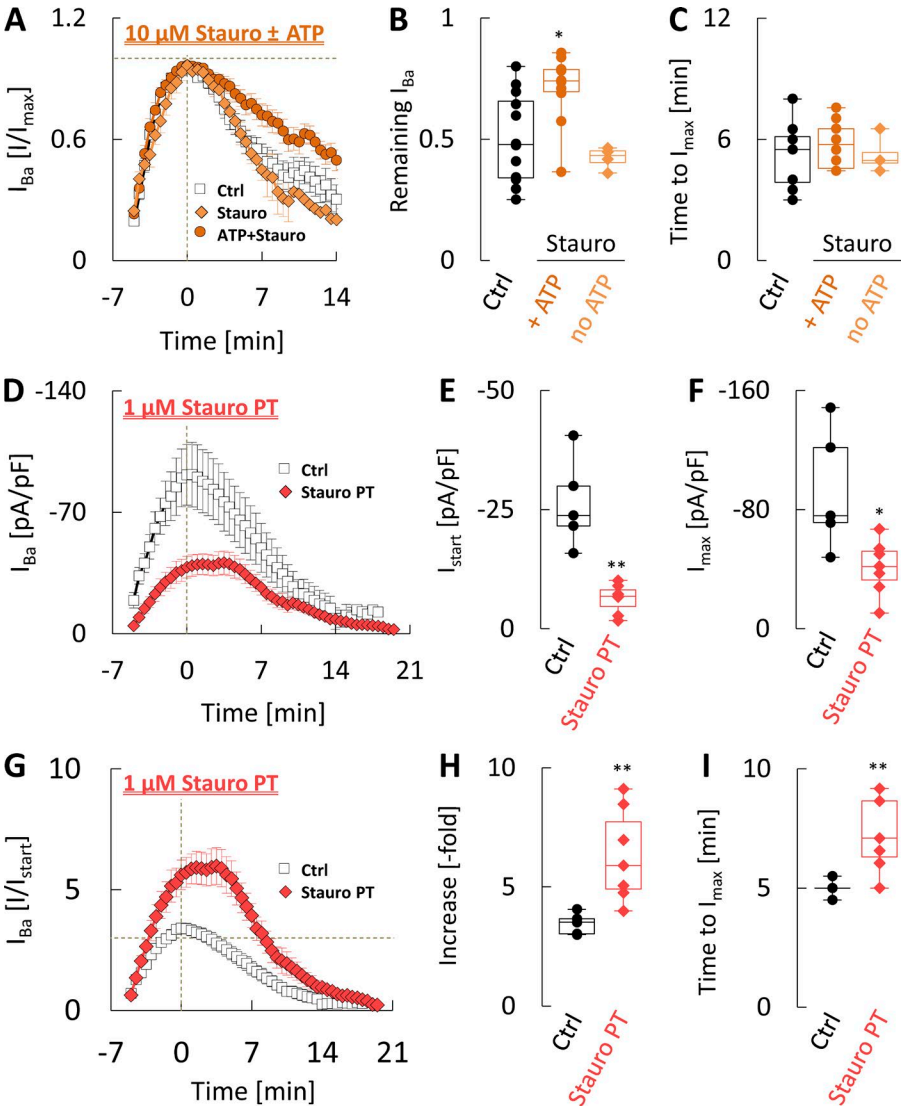

Figure 11. **ATP protection from run-down involves serine/threonine phosphorylation.** **(A)** Mean data from 10 recordings with 5 mM MgATP and 10 µM stauro (ATP+Stauro), 4 recordings with 10 µM stauro only (Stauro), and 12 parallel control recordings (Ctrl). **(B)** Comparison of the residual I_{Ba} after 7 min of run-down in recordings with Stauro or ATP+Stauro and in parallel control recordings (same cells as in A). **(C)** Comparison of the run-up duration in recordings with Stauro or ATP+Stauro and in parallel control recordings (same cells as in A). **(D)** Mean data from seven recordings after pretreatment with 1 µM stauro (Stauro PT) and five parallel control recordings (Ctrl). Note that current amplitudes are expressed in pA/pF to illustrate the reduced peak current densities after stauro pretreatment. **(E)** Comparison of the initial peak current densities observed after stauro pretreatment and in parallel control recordings (same cells as in D). **(F)** Comparison of the maximum peak current densities observed after stauro pretreatment and in parallel control recordings (same cells as in D). **(G)** Same data as in D but normalized to the initial current amplitudes to illustrate changes in the magnitude of run-up. **(H)** Comparison of the current increase during run-up after stauro pretreatment and in parallel control recordings (same cells as in D). **(I)** Comparison of the run-up duration after stauro pretreatment and in parallel control recordings (same cells as in D). *, P < 0.05; **, P < 0.01 (one-way ANOVA with Bonferroni post hoc correction). Values are expressed as mean ± SEM.

biophysical changes could be slowed or prevented by provision of ATP, and this protective action was almost completely abolished by inhibition of serine/threonine kinases. Protein kinase inhibition also mimicked the effects of run-down in intact cells, so it reduced overall peak current densities and hyperpolarized the voltage dependence of gating relative to untreated cells. The effects of ATP could be replicated neither by a nonhydrolyzable ATP analogue nor by GTP, which argues against a role of direct nucleotide binding or G-protein interactions but is consistent with the reported selectivity of protein kinases for ATP (Becher et al., 2013). Finally, run-down was not influenced by dialysis with a PLC inhibitor or the AA scavenger BSA, and the effects of ATP were unaffected by inhibition of lipid kinases, suggesting that run-down was not related to PIP_2 hydrolysis, or accumulation of its cleavage product AA. Based on these findings, we conclude that (1) ATP-protects from $Ca_v2.3$ channel run-down by maintaining phosphorylation of serine/threonine residues on the channels themselves or an associated protein, (2) constitutive dephosphorylation of these sites in dialyzed cells affects channel gating and reduces the total number of functional channels, and (3) (de-)phosphorylation of at least some of the sites can also regulate channel function in intact cells. In addition, some of our findings point to a role of Leu-sensitive proteases for $Ca_v2.3$ channel up-regulation during run-up and for the effects of protein phosphorylation on run-down.

Comparison with run-down in other voltage-gated Ca^{2+} channels

Since its first description, Ca^{2+} channel run-down has been consistently linked to diffusion-controlled dilution of ATP and other cytosolic components, but the underlying processes seem to differ among channels. ATP-induced protection from L-type Ca^{2+} channel run-down involves several interrelated processes, which may include changes in lipid turnover (Wu et al., 2002; Kaur et al., 2015), direct nucleotide binding (Feng et al., 2014), and phosphorylation of the channels by PKA, CaMKII and possibly other kinases (Wang et al., 2009; Xu et al., 2016). The latter counteracts constitutive dephosphorylation by opposing protein phosphatases and has been proposed to stabilize conformations that can be reprimed by voltage, CaM, or calpastatin and/or are more resistant to proteolytic degradation (Chad et al., 1987; Wang et al., 2009; Sun et al., 2014). This is in contrast to the situation

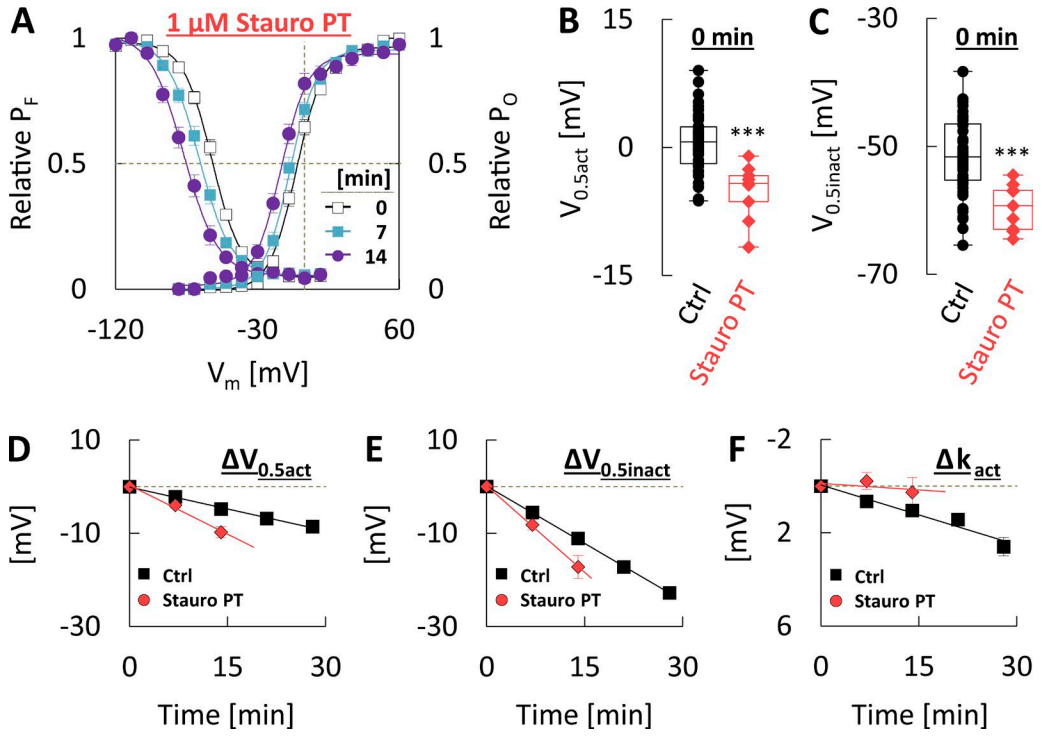

Figure 12. **Protein kinase inhibition in intact cells reproduces the gating changes during run-down in dialyzed cells. (A)** Voltage dependence of activation (right) and prepulse inactivation (left), determined at the onset of run-down (time 0) and in 7-min intervals thereafter in nine cells pretreated with 1 µM stauro for 30–60 min. **(B)** Comparison of half-activation voltages at the onset of run-down in cells pretreated with 1 µM stauro (same cells as in A) and under control conditions (same cells as in Fig. 4). **(C)** Comparison of half-inactivation voltages at the onset of run-down in cells pretreated with 1 µM stauro and under control conditions (same cells as in B). **(D)** Time-course of changes in half-activation voltages during run-down observed in cells pretreated with 1 µM stauro and under control conditions (same cells as in B). **(E)** Time course of changes in half-inactivation voltages during run-down observed in cells pretreated with 1 µM stauro and under control conditions (same cells as in B). **(F)** Time course of changes in activation slope factors during run-down observed in cells pretreated with 1 µM stauro and under control conditions (same cells as in B). ***, P < 0.001 vs. Ctrl (one-way ANOVA with Bonferroni post hoc correction). Values are expressed as mean ± SEM.

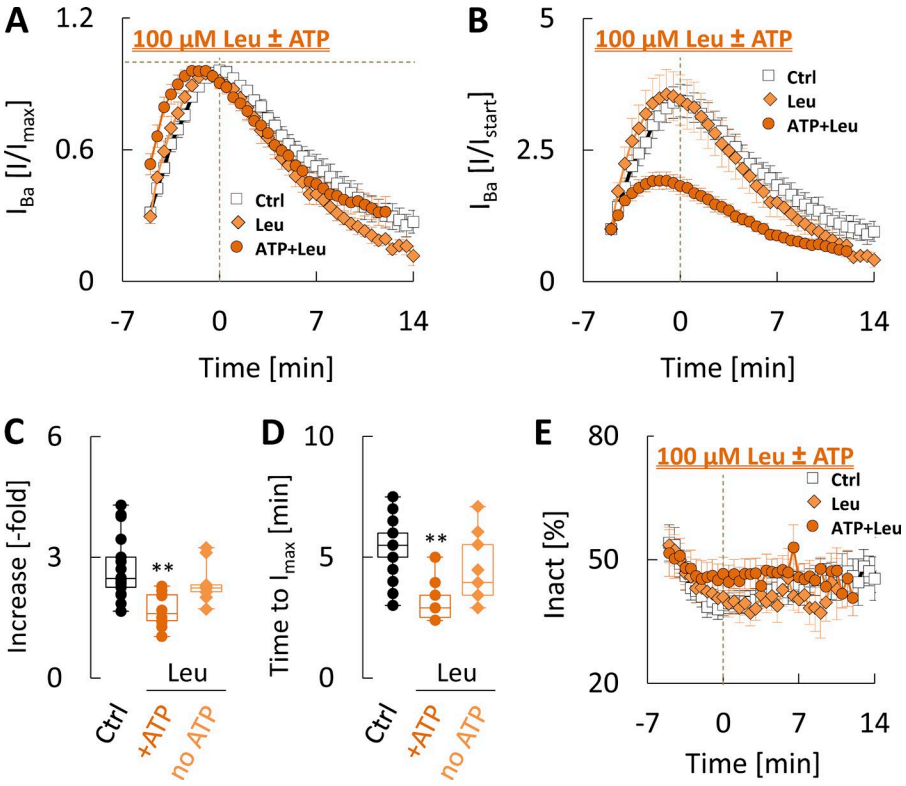

Figure 13. **Run-up may involve activation of Leu-sensitive proteases. (A)** Mean data from 10 recordings with 5 mM MgATP and 100 µM Leu (ATP+Leu), 9 recordings with 100 µM Leu only (Leu), and 17 parallel control recordings (Ctrl). **(B)** Same data as in A but normalized to the initial current amplitude to illustrate differences in the magnitude of run-up. **(C)** Comparison of the current increase during run-up with ATP+Leu, Leu only, and in parallel control recordings (same cells as in A). **(D)** Comparison of the run-up duration with ATP+Leu, Leu only, and in parallel control recordings (same cells as in A). **(E)** Time course of changes in inactivation during the 30-ms test pulses with ATP+Leu, Leu only, and in parallel control recordings (same cells as in A). **, P < 0.01 (one-way ANOVA with Bonferroni post hoc correction in D or Welch's ANOVA with the Games-Howell multiple-comparison method in C). Values are expressed as mean ± SEM.

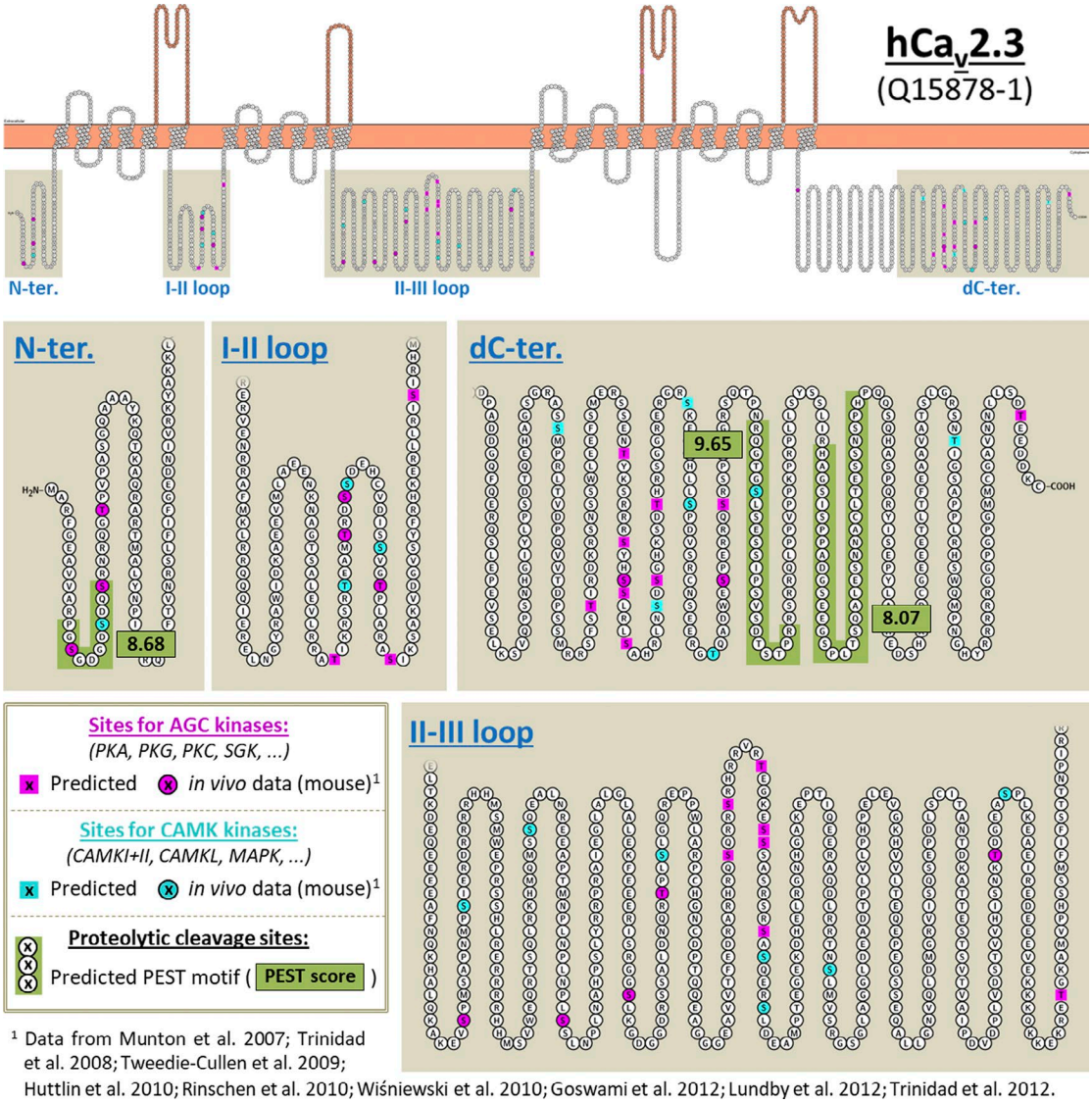

Figure 14. **Phosphorylation sites and potential PEST regions in human $Ca_v2.3$ channels.** The secondary structure was visualized with Protter based on the human protein database entry Q15878, which includes exon 19 and exon 45 encoded stretches of the full-length $Ca_v2.3$d-splice variant. Predictions were performed at the highest threshold by using the Group-based System Software for Prediction of Kinase-specific Phosphorylation Sites 3.0 and at a threshold score of +5.0 by using epestfind for detection of potential proteolytic cleavage sites, respectively. CAMKI, Ca^{2+}/CaM-dependent protein kinase I; CAMKII, Ca^{2+}/CaM-dependent protein kinase II; CAMKL, Ca^{2+}/CaM-dependent protein kinase-like kinases; MAPK, mitogen-activated protein kinase; SGK, serum and glucocorticoid-regulated kinase 1; ter, terminal.

in $Ca_v2.1$ and $Ca_v2.2$ channels, where run-down has been linked to constitutive hydrolysis of membrane PIP_2, which can be prevented by ATP through lipid kinase–mediated PIP_2 resynthesis (Wu et al., 2002; Suh et al., 2010). Although we have not directly tested the effects of PIP_2, our present findings demonstrate that lipid kinases are not involved in ATP-induced protection from $Ca_v2.3$ channel run-down and that the current decline is not related to accumulation of AA. Together with a previous study, where PIP_2-depletion had no effect on $Ca_v2.3$ channels (Suh et al., 2010), these findings argue against a major role of PIP_2 hydrolysis for $Ca_v2.3$ channel run-down. Instead, ATP appears to maintain $Ca_v2.3$ channel function through increased phosphorylation of sites on the channels themselves or an associated protein, which may be required to counteract constitutive dephosphorylation. It has been shown that HEK-293 cells contain endogenous kinases and phosphatases, which can regulate the activity of transfected Ca^{2+} channels (Perez-Reyes et al., 1994; Johnson et al., 1997; Fuller et al., 2010; Aita et al., 2011; Blesneac et al., 2015). In addition, $Ca_v2.3$ channels are a well-known substrate for phosphorylation by various protein kinases (Fig. 14), at least some of which can be constitutively active in HEK-293 cells (Perez-Reyes et al., 1994; Crump et al., 2006). Although no firm conclusions can be drawn with regard to the exact sites or kinases involved in $Ca_v2.3$ channel maintenance, our findings provide a reliable baseline for further studies. They also raise the question how protein phosphorylation might be involved in the maintenance $Ca_v2.1$ and $Ca_v2.2$ channels, which still exhibit significant rundown in the presence of exogenous PIP_2 (Gamper et al., 2004) or with mutations that reduce PIP_2 sensitivity (Zhen et al., 2006). Because there can be cross talk with lipid signaling (Wu et al., 2002) and

PIP_2-hydrolysis partially inhibited $Ca_v2.3$ channels after full activation by PKC (Jeong et al., 2016), it will also be interesting to examine the exact relevance of lipid turnover for this form of regulation.

Molecular mechanisms and potential implications

Very little is known about the molecular and structural mechanisms of Ca^{2+} channel run-down, but possibilities that have been considered include disruption of the linkage between voltage sensors and activation gate, entry into a permanent but existing inactivated state, and spontaneous drops in the total number of channels due to internalization or degradation. Our results do not resolve the exact processes underlying $Ca_v2.3$ channel run-down but do argue against a significant decoupling between voltage-sensors and activation gate because run-down abolished both ionic and gating currents. In addition, Leu was ineffective against run-down and actually reduced the protective effects of ATP, suggesting that the current decline was not directly related to increased proteolytic degradation (but see next section). Together, these findings contrast with studies that L-type–channel gating currents are not diminished by run-down (Hadley and Lederer, 1991; Costantin et al., 1999) and that Leu prevents an irreversible component of run-down in these channels (Chad et al., 1987). We can only speculate that dephosphorylation of $Ca_v2.3$ channels themselves or an interacting protein induces a conformational change that leads to terminal inactivation and/or facilitates their removal from the membrane.

More importantly, our findings reveal that part of the current decline can be attributed to a gradual development of inactivation due to changes in channel voltage dependence. Based on the lack of saturation or concurrent changes in V_{rev}, these effects may have been related to changes in the fraction of applied membrane voltage sensed by the channels. Interestingly, and in contrast to the exponential decline in conductance, the gating changes occurred at a constant rate, which is difficult to reconcile in terms of a conformational change. An attractive hypothesis that remains to be substantiated is that progressive dephosphorylation could shift channels among their states in a simple manner, such as altering the internal surface charge. It has been quantitatively demonstrated that the bulk electrostatic effects of dephosphorylation are sufficient to produce hyperpolarizing voltage shifts during run-down of other voltage-gated ion channels (Perozo and Bezanilla, 1990, 1991). Regardless of the exact mechanism, our findings document a close relationship between protein phosphorylation and channel voltage dependence, which may influence the basal features of current carried by cloned $Ca_v2.3$ channels. Based on previous studies about their native counterparts, it seems reasonable to propose that this is also relevant under physiological conditions. Thus, $Ca_v2.3$ channels are the third most extensively phosphorylated ion channels in mouse brain (Cerda et al., 2011; Fig. 14), and depolarization of intact hippocampal slices has been shown to induce bulk changes in their phosphorylation state (Hell et al., 1995).

Run-up and the role of calpain-like proteases

Unexpectedly, our findings also indicate that $Ca_v2.3$ channel run-up may involve activation of calpain-like proteases (CLPs) and that it can be slowed but not prevented by ATP through increased protein phosphorylation. The process started immediately upon patch rupture, which can hardly be accounted for by ATP depletion but might reflect the loss of small cytosolic protease inhibitors because it was much slower in perforated recordings. In addition, run-up was observed with Ba^{2+} as the charge carrier but significantly faster and more complete with Ca^{2+}, which is consistent with studies that show that Ba^{2+} can partially substitute for Ca^{2+} in activating CLPs (DeMartino and Croall, 1985; McDonald et al., 1994; Seydl et al., 1995). That phosphorylation suppresses most CLPs (Shiraha et al., 2002; Smith et al., 2003), while PIP_2 is well known to be required for activation and may considerably lower their Ca^{2+} requirement (Tompa et al., 2001; Leloup et al., 2010), could explain why (1) ATP, but not AMP-PNP or ATP+stauro, slowed run-up and (2) pretreatment with WM (i.e., partial depletion of membrane PIP_2) further increased the ATP-induced slowing in some cells. Dialysis or pretreatment with stauro alone had no effect or even increased run-up, suggesting that the process was not related to proteolytic activation of protein kinases. With this in mind and considering its fast onset, we can only speculate that run-up might involve partial proteolysis of the channels themselves and/or associated $Ca_v\beta_3$ subunits. Both proteins contain several PEST motifs or PEST-like regions in their C and N termini (Fig. 14), and there is convincing evidence for a functional relevance of these sites as potential cleavage sites. For example, deletion of PEST-like regions in the $Ca_v\beta_3$ subunit increased its half-life, stimulated currents mediated by coexpressed $Ca_v2.2$ channels, and reduced voltage-dependent inactivation in HEK-293 cells (Sandoval et al., 2006). Likewise, intracellular protease application has been shown to produce strong stimulation of VGCCs and a partial loss of fast voltage-dependent inactivation, which has been linked to C-terminal cleavage of a conserved autoinhibitory region in the pore-forming $Ca_v\alpha_1$ subunit (Wei et al., 1994; Klöckner et al., 1995; Gao et al., 2001; Mikala et al., 2003). Given that C-terminal truncation of L-, N- and P/Q-type VGCCs by endogenous proteases has been demonstrated before in HEK-293 cells (Kubodera et al., 2003; Gomez-Ospina et al., 2006) and in vivo (Gerhardstein et al., 2000; Abele and Yang, 2012), it seems not so far off that the structural determinants for $Ca_v2.3$ channel run-up could also be located in this region. With regard to the Leu effects on run-down, it may be important that L-type channels can also be cleaved at PEST regions within the core of the $Ca_v\alpha_1$ subunit, which has been shown to disrupt channel function (Groth et al., 2014; Michailidis et al., 2014). That $Ca_v2.3$ channels lack such regions might account for the inability of Leu to sustain ATP-induced protection. On the other hand, this cannot explain the puzzling finding that Leu actually impaired the protective effects of ATP on run-down. We can only speculate that the latter might be related to differential phosphorylation of long and short forms or changes in the accessibility of certain sites. Because Leu could also alter the effects of ATP in some other way, further studies will clearly be required to delineate the underlying processes. However, our finding that protein kinase inhibition alone replicated most of the gating changes during run-down in intact cells leads us to conclude that proteolysis is either not required for these effects or that it does also occur in intact cells.

Conclusion

In summary, our findings show that run-down of cloned $Ca_v2.3$ channels in dialyzed cells is associated with progressive changes in channel voltage-dependence and a decrease in the total number of functional channels, which can be prevented by ATP through maintained protein phosphorylation and replicated by protein kinase inhibition in intact cells. These findings distinguish the process from run-down in other Ca_v2 channels and suggest that one or more sites on the channels themselves or an associated protein must be phosphorylated to maintain them in a functional state. In addition, changes in the phosphorylation of a subset of sites may directly influence channel gating, possibly through bulk electrostatics. Although additional studies will be required to delineate the underlying mechanisms and their relevance in native cells, our results provide a reliable baseline that could stimulate further work on $Ca_v2.3$ channel regulation by protein kinases, phosphatases, and possibly proteases.

Acknowledgments

We thank Tobias Pook for technical help and supply of software for facilitated analysis and Mrs. Renate Clemens for her excellent and permanent assistance.

This work was financially supported by the Deutsche Forschungsgemeinschaft (SCHN 387/21-1).

The authors declare no competing financial interests.

Author contributions: F. Neumaier contributed to the conception and design of the work, performed the experiments, analyzed and interpreted the data, prepared the figures, wrote the first draft of the manuscript, and coordinated its critical revision. T. Schneider contributed to the conception and design of the work, interpretation of the data, and critical revision of the manuscript. S. Alpdogan and J. Hescheler contributed to analysis and interpretation of the data and drafting of the manuscript. All authors have approved the final version of the manuscript and agree to be accountable for all aspects of the work. All persons designated as authors qualify for authorship, and all those who qualify for authorship are listed. Experiments were carried out in the Institute for Neurophysiology at the University of Cologne, Germany.

Sharona E. Gordon served as editor.

Submitted: 14 August 2017
Revised: 22 December 2017
Accepted: 24 January 2018

References

Abele, K., and J. Yang. 2012. Regulation of voltage-gated calcium channels by proteolysis. *Sheng Li Xue Bao.* 64:504–514.

Aita, Y., N. Kurebayashi, S. Hirose, and A.D. Maturana. 2011. Protein kinase D regulates the human cardiac L-type voltage-gated calcium channel through serine 1884. *FEBS Lett.* 585:3903–3906. https://doi.org/10.1016/j.febslet.2011.11.011

Almog, M., and A. Korngreen. 2009. Characterization of voltage-gated Ca^{2+} conductances in layer 5 neocortical pyramidal neurons from rats. *PLoS One.* 4:e4841. https://doi.org/10.1371/journal.pone.0004841

Armstrong, D., and R. Eckert. 1987. Voltage-activated calcium channels that must be phosphorylated to respond to membrane depolarization. *Proc. Natl. Acad. Sci. USA.* 84:2518–2522. https://doi.org/10.1073/pnas.84.8.2518

Arnould, T., D. Janssens, C. Michiels, and J. Remacle. 1996. Effect of aescine on hypoxia-induced activation of human endothelial cells. *Eur. J. Pharmacol.* 315:227–233. https://doi.org/10.1016/S0014-2999(96)00645-0

Becher, I., M.M. Savitski, M.F. Savitski, C. Hopf, M. Bantscheff, and G. Drewes. 2013. Affinity profiling of the cellular kinome for the nucleotide cofactors ATP, ADP, and GTP. *ACS Chem. Biol.* 8:599–607. https://doi.org/10.1021/cb3005879

Becq, F. 1996. Ionic channel rundown in excised membrane patches. *Biochim. Biophys. Acta.* 1286:53–63. https://doi.org/10.1016/0304-4157(96)00002-0

Benquet, P., J.L. Guen, G. Dayanithi, Y. Pichon, and F. Tiaho. 1999. omega-AgaI-VA-sensitive (P/Q-type) and -resistant (R-type) high-voltage-activated Ba(2+) currents in embryonic cockroach brain neurons. *J. Neurophysiol.* 82:2284–2293. https://doi.org/10.1152/jn.1999.82.5.2284

Blesneac, I., J. Chemin, I. Bidaud, S. Huc-Brandt, F. Vandermoere, and P. Lory. 2015. Phosphorylation of the $Ca_v3.2$ T-type calcium channel directly regulates its gating properties. *Proc. Natl. Acad. Sci. USA.* 112:13705–13710. https://doi.org/10.1073/pnas.1511740112

Cerda, O., J.-H. Baek, and J.S. Trimmer. 2011. Mining recent brain proteomic databases for ion channel phosphosite nuggets. *J. Gen. Physiol.* 137:3–16. https://doi.org/10.1085/jgp.201010555

Chad, J.E., and R. Eckert. 1986. An enzymatic mechanism for calcium current inactivation in dialysed Helix neurones. *J. Physiol.* 378:31–51. https://doi.org/10.1113/jphysiol.1986.sp016206

Chad, J., D. Kalman, and D. Armstrong. 1987. The role of cyclic AMP-dependent phosphorylation in the maintenance and modulation of voltage-activated calcium channels. *Soc. Gen. Physiol. Ser.* 42:167–186.

Clare, J.J. 2006. Functional expression of ion channels in mammalian systems. *In* Expression and Analysis of Recombinant Ion Channels. J.J. Clare and D.J. Trezise, editors. Wiley-VCH, Weinheim, Germany. 79–109.

Costantin, J.L., N. Qin, M.N. Waxham, L. Birnbaumer, and E. Stefani. 1999. Complete reversal of run-down in rabbit cardiac Ca^{2+} channels by patch-cramming in Xenopus oocytes; partial reversal by protein kinase A. *Pflugers Arch.* 437:888–894. https://doi.org/10.1007/s004240050859

Cota, G. 1986. Calcium channel currents in pars intermedia cells of the rat pituitary gland. Kinetic properties and washout during intracellular dialysis. *J. Gen. Physiol.* 88:83–105. https://doi.org/10.1085/jgp.88.1.83

Crump, S.M., R.N. Correll, E.A. Schroder, W.C. Lester, B.S. Finlin, D.A. Andres, and J. Satin. 2006. L-type calcium channel alpha-subunit and protein kinase inhibitors modulate Rem-mediated regulation of current. *Am. J. Physiol. Heart Circ. Physiol.* 291:H1959–H1971. https://doi.org/10.1152/ajpheart.00956.2005

DeMartino, G.N., and D.E. Croall. 1985. Calcium-dependent proteases from liver and heart. *Prog. Clin. Biol. Res.* 180:117–126.

Elhamdani, A., J.-L. Bossu, and A. Feltz. 1994. Evolution of the Ca^{2+} current during dialysis of isolated bovine chromaffin cells: effect of internal calcium. *Cell Calcium.* 16:357–366. https://doi.org/10.1016/0143-4160(94)90029-9

Elhamdani, A., J.-L. Bossu, and A. Feltz. 1995. ATP and G proteins affect the runup of the Ca^{2+} current in bovine chromaffin cells. *Pflugers Arch.* 430:410–419. https://doi.org/10.1007/BF00373917

Fan, J.-S., and P. Palade. 1998. Perforated patch recording with beta-escin. *Pflugers Arch.* 436:1021–1023. https://doi.org/10.1007/PL00008086

Feng, R., J. Xu, E. Minobe, A. Kameyama, L. Yang, L. Yu, L. Hao, and M. Kameyama. 2014. Adenosine triphosphate regulates the activity of guinea pig $Ca_v1.2$ channel by direct binding to the channel in a dose-dependent manner. *Am. J. Physiol. Cell Physiol.* 306:C856–C863. https://doi.org/10.1152/ajpcell.00368.2013

Fomina, A.F., and E.S. Levitan. 1997. Control of Ca^{2+} channel current and exocytosis in rat lactotrophs by basally active protein kinase C and calcineurin. *Neuroscience.* 78:523–531. https://doi.org/10.1016/S0306-4522(96)00571-4

Fu, L.-Y., F. Wang, X.-S. Chen, H.-Y. Zhou, W.-X. Yao, G.-J. Xia, and M.-X. Jiang. 2003. Perforated patch recording of L-type calcium current with beta-escin in guinea pig ventricular myocytes. *Acta Pharmacol. Sin.* 24:1094–1098.

Fuller, M.D., M.A. Emrick, M. Sadilek, T. Scheuer, and W.A. Catterall. 2010. Molecular mechanism of calcium channel regulation in the fight-or-flight response. *Sci. Signal.* 3:ra70. https://doi.org/10.1126/scisignal.2001152

Gamper, N., V. Reznikov, Y. Yamada, J. Yang, and M.S. Shapiro. 2004. Phosphatidylinositol [correction] 4,5-bisphosphate signals underlie

receptor-specific Gq/11-mediated modulation of N-type Ca2+ channels. *J. Neurosci.* 24:10980–10992. https://doi.org/10.1523/JNEUROSCI.3869-04.2004

Gao, T., A.E. Cuadra, H. Ma, M. Bunemann, B.L. Gerhardstein, T. Cheng, R.T. Eick, and M.M. Hosey. 2001. C-terminal fragments of the alpha 1C ($Ca_V1.2$) subunit associate with and regulate L-type calcium channels containing C-terminal-truncated alpha 1C subunits. *J. Biol. Chem.* 276:21089–21097. https://doi.org/10.1074/jbc.M008000200

Gerhardstein, B.L., T. Gao, M. Bünemann, T.S. Puri, A. Adair, H. Ma, and M.M. Hosey. 2000. Proteolytic processing of the C terminus of the alpha(1C) subunit of L-type calcium channels and the role of a proline-rich domain in membrane tethering of proteolytic fragments. *J. Biol. Chem.* 275:8556–8563. https://doi.org/10.1074/jbc.275.12.8556

Gomez-Ospina, N., F. Tsuruta, O. Barreto-Chang, L. Hu, and R. Dolmetsch. 2006. The C terminus of the L-type voltage-gated calcium channel $Ca_V1.2$ encodes a transcription factor. *Cell.* 127:591–606. https://doi.org/10.1016/j.cell.2006.10.017

Goswami, T., X. Li, A.M. Smith, E.M. Luderowski, J.J. Vincent, J. Rush, and B.A. Ballif. 2012. Comparative phosphoproteomic analysis of neonatal and adult murine brain. *Proteomics.* 12:2185–2189. https://doi.org/10.1002/pmic.201200003

Groth, R.D., N.N. Tirko, and R.W. Tsien. 2014. $Ca_V1.2$ calcium channels: Just cut out to be regulated? *Neuron.* 82:939–940. https://doi.org/10.1016/j.neuron.2014.05.030

Hadley, R.W., and W.J. Lederer. 1991. Properties of L-type calcium channel gating current in isolated guinea pig ventricular myocytes. *J. Gen. Physiol.* 98:265–285. https://doi.org/10.1085/jgp.98.2.265

Hamill, O.P., A. Marty, E. Neher, B. Sakmann, and F.J. Sigworth. 1981. Improved patch-clamp techniques for high-resolution current recording from cells and cell-free membrane patches. *Pflugers Arch.* 391:85–100. https://doi.org/10.1007/BF00656997

Hell, J.W., C.T. Yokoyama, L.J. Breeze, C. Chavkin, and W.A. Catterall. 1995. Phosphorylation of presynaptic and postsynaptic calcium channels by cAMP-dependent protein kinase in hippocampal neurons. *EMBO J.* 14:3036–3044.

Hilaire, C., S. Diochot, G. Desmadryl, S. Richard, and J. Valmier. 1997. Toxin-resistant calcium currents in embryonic mouse sensory neurons. *Neuroscience.* 80:267–276. https://doi.org/10.1016/S0306-4522(97)00101-2

Hilgemann, D.W. 1997. Cytoplasmic ATP-dependent regulation of ion transporters and channels: Mechanisms and messengers. *Annu. Rev. Physiol.* 59:193–220. https://doi.org/10.1146/annurev.physiol.59.1.193

Horváth, F., L. Erdei, B. Wodala, U. Homann, and G. Thiel. 2002. Deltamethrin rescues run down of K^+ outward rectifying channels in Vicia faba guard cells. *Acta Biol. Szeged.* 46:19–20.

Huttlin, E.L., M.P. Jedrychowski, J.E. Elias, T. Goswami, R. Rad, S.A. Beausoleil, J. Villén, W. Haas, M.E. Sowa, and S.P. Gygi. 2010. A tissue-specific atlas of mouse protein phosphorylation and expression. *Cell.* 143:1174–1189. https://doi.org/10.1016/j.cell.2010.12.001

Jeong, J.-Y., H.-J. Kweon, and B.-C. Suh. 2016. Dual regulation of R-type Cav2.3 channels by M_1 muscarinic receptors. *Mol. Cells.* 39:322–329. https://doi.org/10.14348/molcells.2016.2292

Johnson, B.D., J.P. Brousal, B.Z. Peterson, P.A. Gallombardo, G.H. Hockerman, Y. Lai, T. Scheuer, and W.A. Catterall. 1997. Modulation of the cloned skeletal muscle L-type Ca^{2+} channel by anchored cAMP-dependent protein kinase. *J. Neurosci.* 17:1243–1255.

Kaur, G., A. Pinggera, N.J. Ortner, A. Lieb, M.J. Sinnegger-Brauns, V. Yarov-Yarovoy, G.J. Obermair, B.E. Flucher, and J. Striessnig. 2015. A polybasic plasma membrane binding motif in the I-II linker stabilizes voltage-gated $Ca_V1.2$ calcium channel function. *J. Biol. Chem.* 290:21086–21100. https://doi.org/10.1074/jbc.M115.645671

Kepplinger, K.J.F., and C. Romanin. 2005. The run-down phenomenon of Ca2+ channels. *In* Voltage-Gated Calcium Channels. Springer, Boston. 219–230.

Klöckner, U., G. Mikala, M. Varadi, G. Varadi, and A. Schwartz. 1995. Involvement of the carboxyl-terminal region of the α_1 subunit in voltage-dependent inactivation of cardiac calcium channels. *J. Biol. Chem.* 270:17306–17310. https://doi.org/10.1074/jbc.270.29.17306

Kubodera, T., T. Yokota, K. Ohwada, K. Ishikawa, H. Miura, T. Matsuoka, and H. Mizusawa. 2003. Proteolytic cleavage and cellular toxicity of the human α1A calcium channel in spinocerebellar ataxia type 6. *Neurosci. Lett.* 341:74–78. https://doi.org/10.1016/S0304-3940(03)00156-3

Leloup, L., H. Shao, Y.H. Bae, B. Deasy, D. Stolz, P. Roy, and A. Wells. 2010. m-Calpain activation is regulated by its membrane localization and by its binding to phosphatidylinositol 4,5-bisphosphate. *J. Biol. Chem.* 285:33549–33566. https://doi.org/10.1074/jbc.M110.123604

Liu, L., and A.R. Rittenhouse. 2003. Arachidonic acid mediates muscarinic inhibition and enhancement of N-type Ca^{2+} current in sympathetic neurons. *Proc. Natl. Acad. Sci. USA.* 100:295–300. https://doi.org/10.1073/pnas.0136826100

Liu, L., C.F. Barrett, and A.R. Rittenhouse. 2001. Arachidonic acid both inhibits and enhances whole cell calcium currents in rat sympathetic neurons. *Am. J. Physiol. Cell Physiol.* 280:C1293–C1305. https://doi.org/10.1152/ajpcell.2001.280.5.C1293

Liu, L., R. Zhao, Y. Bai, L.F. Stanish, J.E. Evans, M.J. Sanderson, J.V. Bonventre, and A.R. Rittenhouse. 2006. M_1 muscarinic receptors inhibit L-type Ca^{2+} current and M-current by divergent signal transduction cascades. *J. Neurosci.* 26:11588–11598. https://doi.org/10.1523/JNEUROSCI.2102-06.2006

Lundby, A., A. Secher, K. Lage, N.B. Nordsborg, A. Dmytriyev, C. Lundby, and J.V. Olsen. 2012. Quantitative maps of protein phosphorylation sites across 14 different rat organs and tissues. *Nat. Commun.* 3:876. https://doi.org/10.1038/ncomms1871

McDonald, T.F., S. Pelzer, W. Trautwein, and D.J. Pelzer. 1994. Regulation and modulation of calcium channels in cardiac, skeletal, and smooth muscle cells. *Physiol. Rev.* 74:365–507. https://doi.org/10.1152/physrev.1994.74.2.365

Michailidis, I.E., K. Abele-Henckels, W.K. Zhang, B. Lin, Y. Yu, L.S. Geyman, M.D. Ehlers, E.A. Pnevmatikakis, and J. Yang. 2014. Age-related homeostatic midchannel proteolysis of neuronal L-type voltage-gated Ca^{2+} channels. *Neuron.* 82:1045–1057. https://doi.org/10.1016/j.neuron.2014.04.017

Mikala, G., I. Bodi, U. Klöckner, M. Varadi, G. Varadi, S.E. Koch, and A. Schwartz. 2003. Characterization of auto-regulation of the human cardiac α_1 subunit of the L-type calcium channel: importance of the C-terminus. *Mol. Cell. Biochem.* 250:81–89. https://doi.org/10.1023/A:1024910605389

Munton, R.P., R. Tweedie-Cullen, M. Livingstone-Zatchej, F. Weinandy, M. Waidelich, D. Longo, P. Gehrig, F. Potthast, D. Rutishauser, B. Gerrits, et al. 2007. Qualitative and quantitative analyses of protein phosphorylation in naive and stimulated mouse synaptosomal preparations. *Mol. Cell. Proteomics.* 6:283–293. https://doi.org/10.1074/mcp.M600046-MCP200

Nakashima, Y.M., S.M. Todorovic, A. Pereverzev, J. Hescheler, T. Schneider, and C.J. Lingle. 1998. Properties of Ba2+ currents arising from human α1E and α1Ebeta3 constructs expressed in HEK293 cells: Physiology, pharmacology, and comparison to native T-type Ba2+ currents. *Neuropharmacology.* 37:957–972. https://doi.org/10.1016/S0028-3908(98)00097-5

Omasits, U., C.H. Ahrens, S. Müller, and B. Wollscheid. 2014. Protter: Interactive protein feature visualization and integration with experimental proteomic data. *Bioinformatics.* 30:884–886. https://doi.org/10.1093/bioinformatics/btt607

Park, S.W., D. Byun, Y.M. Bae, B.H. Choi, S.H. Park, B. Kim, and S.I. Cho. 2007. Effects of fluid flow on voltage-dependent calcium channels in rat vascular myocytes: fluid flow as a shear stress and a source of artifacts during patch-clamp studies. *Biochem. Biophys. Res. Commun.* 358:1021–1027. https://doi.org/10.1016/j.bbrc.2007.05.024

Peng, S.Q., R.K. Hajela, and W.D. Atchison. 2005. Fluid flow-induced increase in inward Ba^{2+} current expressed in HEK293 cells transiently transfected with human neuronal L-type Ca^{2+} channels. *Brain Res.* 1045:116–123. https://doi.org/10.1016/j.brainres.2005.03.039

Perez-Reyes, E., W. Yuan, X. Wei, and D.M. Bers. 1994. Regulation of the cloned L-type cardiac calcium channel by cyclic-AMP-dependent protein kinase. *FEBS Lett.* 342:119–123. https://doi.org/10.1016/0014-5793(94)80484-2

Perozo, E., and F. Bezanilla. 1990. Phosphorylation affects voltage gating of the delayed rectifier K^+ channel by electrostatic interactions. *Neuron.* 5:685–690. https://doi.org/10.1016/0896-6273(90)90222-2

Perozo, E., and F. Bezanilla. 1991. Phosphorylation of K^+ channels in the squid giant axon. A mechanistic analysis. *J. Bioenerg. Biomembr.* 23:599–613. https://doi.org/10.1007/BF00785813

Rinschen, M.M., M.-J. Yu, G. Wang, E.S. Boja, J.D. Hoffert, T. Pisitkun, and M.A. Knepper. 2010. Quantitative phosphoproteomic analysis reveals vasopressin V2-receptor-dependent signaling pathways in renal collecting duct cells. *Proc. Natl. Acad. Sci. USA.* 107:3882–3887. https://doi.org/10.1073/pnas.0910646107

Sandoval, A., N. Oviedo, A. Tadmouri, T. Avila, M. De Waard, and R. Felix. 2006. Two PEST-like motifs regulate Ca2+/calpain-mediated cleavage of the CaVbeta3 subunit and provide important determinants for neuronal Ca2+ channel activity. *Eur. J. Neurosci.* 23:2311–2320. https://doi.org/10.1111/j.1460-9568.2006.04749.x

Seydl, K., J.-O. Karlsson, A. Dominik, H. Gruber, and C. Romanin. 1995. Action of calpastatin in prevention of cardiac L-type Ca^{2+} channel run-down cannot be mimicked by synthetic calpain inhibitors. *Pflugers Arch.* 429:503–510. https://doi.org/10.1007/BF00704155

Shiraha, H., A. Glading, J. Chou, Z. Jia, and A. Wells. 2002. Activation of m-calpain (calpain II) by epidermal growth factor is limited by protein kinase A phosphorylation of m-calpain. *Mol. Cell. Biol.* 22:2716–2727. https://doi.org/10.1128/MCB.22.8.2716-2727.2002

Smith, S.D., Z. Jia, K.K. Huynh, A. Wells, and J.S. Elce. 2003. Glutamate substitutions at a PKA consensus site are consistent with inactivation of calpain by phosphorylation. *FEBS Lett.* 542:115–118. https://doi.org/10.1016/S0014-5793(03)00361-2

Suh, B.-C., K. Leal, and B. Hille. 2010. Modulation of high-voltage activated Ca^{2+} channels by membrane phosphatidylinositol 4,5-bisphosphate. *Neuron.* 67:224–238. https://doi.org/10.1016/j.neuron.2010.07.001

Sun, W., R. Feng, H. Hu, F. Guo, Q. Gao, D. Shao, D. Yin, H. Wang, X. Sun, M. Zhao, et al. 2014. The Ca^{2+}-dependent interaction of calpastatin domain L with the C-terminal tail of the $Ca_V1.2$ channel. *FEBS Lett.* 588:665–671. https://doi.org/10.1016/j.febslet.2014.01.019

Thomas, P., and T.G. Smart. 2005. HEK293 cell line: A vehicle for the expression of recombinant proteins. *J. Pharmacol. Toxicol. Methods.* 51:187–200. https://doi.org/10.1016/j.vascn.2004.08.014

Tiaho, F., J. Nargeot, and S. Richard. 1993. Repriming of L-type calcium currents revealed during early whole-cell patch-clamp recordings in rat ventricular cells. *J. Physiol.* 463:367–389. https://doi.org/10.1113/jphysiol.1993.sp019599

Tompa, P., R. Töth-Boconádi, and P. Friedrich. 2001. Frequency decoding of fast calcium oscillations by calpain. *Cell Calcium.* 29:161–170. https://doi.org/10.1054/ceca.2000.0179

Toth, P.T., L.R. Shekter, G.H. Ma, L.H. Philipson, and R.J. Miller. 1996. Selective G-protein regulation of neuronal calcium channels. *J. Neurosci.* 16:4617–4624.

Trinidad, J.C., A. Thalhammer, C.G. Specht, A.J. Lynn, P.R. Baker, R. Schoepfer, and A.L. Burlingame. 2008. Quantitative analysis of synaptic phosphorylation and protein expression. *Mol. Cell. Proteomics.* 7:684–696. https://doi.org/10.1074/mcp.M700170-MCP200

Trinidad, J.C., D.T. Barkan, B.F. Gulledge, A. Thalhammer, A. Sali, R. Schoepfer, and A.L. Burlingame. 2012. Global identification and characterization of both O-GlcNAcylation and phosphorylation at the murine synapse. *Mol. Cell. Proteomics.* 11:215–229. https://doi.org/10.1074/mcp.O112.018366

Tweedie-Cullen, R.Y., J.M. Reck, and I.M. Mansuy. 2009. Comprehensive mapping of post-translational modifications on synaptic, nuclear, and histone proteins in the adult mouse brain. *J. Proteome Res.* 8:4966–4982. https://doi.org/10.1021/pr9003739

Wang, W.-Y., L.-Y. Hao, E. Minobe, Z.A. Saud, D.-Y. Han, and M. Kameyama. 2009. CaMKII phosphorylates a threonine residue in the C-terminal tail of $Ca_V1.2$ Ca^{2+} channel and modulates the interaction of the channel with calmodulin. *J. Physiol. Sci.* 59:283–290. https://doi.org/10.1007/s12576-009-0033-y

Wei, X., A. Neely, A.E. Lacerda, R. Olcese, E. Stefani, E. Perez-Reyes, and L. Birnbaumer. 1994. Modification of Ca^{2+} channel activity by deletions at the carboxyl terminus of the cardiac α_1 subunit. *J. Biol. Chem.* 269:1635–1640.

Wipf, P., and R.J. Halter. 2005. Chemistry and biology of wortmannin. *Org. Biomol. Chem.* 3:2053–2061. https://doi.org/10.1039/b504418a

Wiśniewski, J.R., N. Nagaraj, A. Zougman, F. Gnad, and M. Mann. 2010. Brain phosphoproteome obtained by a FASP-based method reveals plasma membrane protein topology. *J. Proteome Res.* 9:3280–3289. https://doi.org/10.1021/pr1002214

Wu, L., C.S. Bauer, X.-G. Zhen, C. Xie, and J. Yang. 2002. Dual regulation of voltage-gated calcium channels by $PtdIns(4,5)P_2$. *Nature.* 419:947–952. https://doi.org/10.1038/nature01118

Xu, J., L. Yu, E. Minobe, L. Lu, M. Lei, and M. Kameyama. 2016. PKA and phosphatases attached to the $Ca_V1.2$ channel regulate channel activity in cell-free patches. *Am. J. Physiol. Cell Physiol.* 310:C136–C141. https://doi.org/10.1152/ajpcell.00157.2015

Xue, Y., J. Ren, X. Gao, C. Jin, L. Wen, and X. Yao. 2008. GPS 2.0, a tool to predict kinase-specific phosphorylation sites in hierarchy. *Mol. Cell. Proteomics.* 7:1598–1608. https://doi.org/10.1074/mcp.M700574-MCP200

Yu, L., J. Xu, E. Minobe, A. Kameyama, L. Yang, R. Feng, L. Hao, and M. Kameyama. 2016. Role of protein phosphatases in the run down of guinea pig cardiac $Ca_V1.2$ Ca^{2+} channels. *Am. J. Physiol. Cell Physiol.* 310:C773–C779. https://doi.org/10.1152/ajpcell.00199.2015

Zhang, H., L.C. Craciun, T. Mirshahi, T. Rohács, C.M. Lopes, T. Jin, and D.E. Logothetis. 2003. PIP_2 activates KCNQ channels, and its hydrolysis underlies receptor-mediated inhibition of M currents. *Neuron.* 37:963–975. https://doi.org/10.1016/S0896-6273(03)00125-9

Zhen, X.-G., C. Xie, Y. Yamada, Y. Zhang, C. Doyle, and J. Yang. 2006. A single amino acid mutation attenuates rundown of voltage-gated calcium channels. *FEBS Lett.* 580:5733–5738. https://doi.org/10.1016/j.febslet.2006.09.027